

Resonance-dominant optomechanical entanglement in open quantum systems

Cheng Shang^{1,2,*} and Hongchao Li^{3,†}

¹Department of Physics, The University of Tokyo, 5-1-5 Kashiwanoha, Kashiwa, Chiba 277-8574, Japan

²Analytical Quantum Complexity RIKEN Hakubi Research Team, RIKEN Center for Quantum Computing (RQC), 2-1 Hirosawa, Wako, Saitama 351-0198, Japan

³Department of Physics, The University of Tokyo, 7-3-1 Hongo, Tokyo 113-0033, Japan

(Received 10 November 2023; revised 28 February 2024; accepted 29 March 2024; published 25 April 2024)

Motivated by entanglement protection, our work utilizes a resonance effect to enhance optomechanical entanglement in the coherent-state representation. We propose a filtering model to filter out the significant detuning components between a thermal-mechanical mode and its surrounding heat baths in the weak-coupling limit. We reveal that protecting continuous-variable entanglement involves the elimination of degrees of freedom associated with significant detuning components, thereby resisting decoherence. We construct a nonlinear Langevin equation of the filtering model and numerically show that the filtering model doubles the robustness of the stationary maximum optomechanical entanglement to the thermal fluctuation noise and mechanical damping. Furthermore, we generalize these results to an optical cavity array with one oscillating end mirror to investigate the long-distance optimal optomechanical-entanglement transfer. Our study breaks new ground for applying the resonance effect to protect quantum systems from decoherence and advancing the possibilities of large-scale quantum information processing and quantum network construction.

DOI: 10.1103/PhysRevApplied.21.044048

I. INTRODUCTION

Entanglement is an essential feature of quantum systems and one of the most striking phenomena of quantum theory [1], allowing for inseparable quantum correlations shared by distant parties [2]. Entanglement is crucial in quantum information processing and network building [3–5]. Studying entanglement properties from the perspectives of discrete and continuous variables is significant for further understanding the quantum-classical correspondence [6,7]. So far, the bipartite entanglement for a microscopic system of discrete variables with a few degrees of freedom has been studied in detail [8]. A primary example of this is a two-qubit system. To quantify entanglement, concurrence [9], negativity [10], or the von Neumann entropy [11] are frequently used in previous studies.

Nevertheless, exploring bipartite entanglement in a macroscopic system of continuous variables with a large number of degrees of freedom has remained elusive [12–15]. Unfortunately, entanglement is fragile due to decoherence from inevitable dissipative couplings between an entangled system and its surrounding environment. Therefore, generating, measuring, and protecting entanglement in open quantum systems have raised widespread interest

in various branches of physics and have been expected to be demonstrated to date [16].

Cavity optomechanical systems are based on couplings due to radiation pressure between electromagnetic and mechanical degrees of freedom [17]. They provide a desirable mesoscopic platform for studying continuous-variable entanglement between optical cavity fields and macroscopic mechanical oscillators with vast degrees of freedom in open quantum systems [18,19]. Thanks to the rapidly developing field of microfabrication, quantum effects are becoming more significant as the size of devices is shrinking [20–25]. Remarkable progress has been made in generating entanglement by manipulating macroscopic nanomechanical oscillators with high precision [26,27]. Some landmark contributions have been achieved for an optomechanical-entanglement measure [28,29], such as using logarithmic negativity to calculate an upper bound of distillable optomechanical entanglement [30].

Protecting the maximum optomechanical entanglement in open quantum systems has recently become a research focus. Many schemes have been proposed, such as protecting entanglement via synthetic magnetism in loop-coupled cavity optomechanical systems from thermal noise and dark mode [31], realizing phase-controlled asymmetric entanglement in cavity optomechanical systems of whispering-gallery mode [32], achieving and preserving the optimal quality of nonreciprocal

*Corresponding author: c-shang@iis.u-tokyo.ac.jp

†Corresponding author: lhc@cat.phys.s.u-tokyo.ac.jp

optomechanical entanglement via the Sagnac effect in a spinning cavity optomechanical system evanescently coupled with a tapered fiber [33,34], and via general dark-mode control to accomplish thermal-noise-resistant entanglement [35].

However, the auxiliary protection of optomechanical entanglement in these schemes all work in hybrid cavity optomechanical systems, which inevitably brings about trilateral and even multilateral entanglement problems [36], such as photon-phonon-atom entanglement [37]. In this sense, it is essential to develop methods of protecting the intrinsic bilateral optomechanical entanglement in hybrid cavity optomechanical systems from potential interference caused by additional types of degrees of freedom [38]. With this motivation, we aim to protect a prototypical optomechanical entanglement in cavity optomechanical systems.

Currently, intriguing schemes have been proposed to achieve the frequency resonance of the system by using laser driving, thereby protecting bilateral mechanical entanglement in doubly resonant cavity optomechanical systems [39,40] and photon-atom entanglement in the Rabi model [41]. Inspired by this, we propose to utilize the high-frequency resonance effect in a Fabry-Perot cavity to protect the maximal value of optomechanical entanglement. In the weak-coupling limit, a clearcut physical mechanism is employed to reduce Brownian noise and dissipation, which involves filtering out components with significant mismatched coupling frequencies between a mechanical mode and its thermal reservoir by leveraging the high-frequency resonance effect. The present theoretical conjecture can be materialized in an experiment by laser driving the optical cavity field to resonate with a high-frequency and high-quality-factor mechanical resonator coupled to a Markovian structured environment. We can observe resonance-dominant optomechanical entanglement using a homodyne detection scheme [42,43] or a cavity-assisted measurement scheme [44,45].

To attain our goal, we start by constructing the Hamiltonian of the cavity optomechanical system under the coherent-state representation. We then derive its associated nonlinear Langevin equations, which are consistent with the results in Ref. [28] but originate from the coherent-state representation. We finally propose a theory of resonance-dominant optomechanical entanglement in continuous-variable systems. When the mechanical mode and surrounding heat baths satisfy the conditions of weak coupling and high-frequency resonance, we point out that the filtering model protects the stationary maximum optomechanical entanglement. In particular, we quantitatively observe that a resonance effect doubles the robustness of the mechanical damping and thermal fluctuation noise from the environment and reveals its physical reason. This result first unveils a hitherto overlooked aspect of applying a resonance effect to entanglement protection.

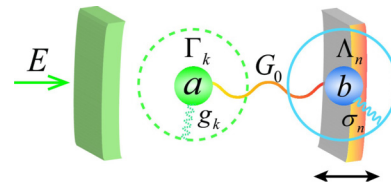


FIG. 1. A cavity optomechanical system driven by a monochromatic laser. The optical and mechanical modes are coupled via radiation pressure while independently coupled to their respective reservoirs.

We further extend these results to an array of optical cavities with one oscillating end mirror and investigate the remote optomechanical entanglement, which helps achieve optimal optomechanical entanglement transmission for quantum information processing.

The remainder of this paper is organized as follows. In Sec. II, we construct the Hamiltonian of the physical system and reproduce the results of nonlinear Langevin equations in Ref. [28] in the coherent-state representation. In Sec. III, we propose a theory of resonance-dominant optomechanical entanglement in continuous-variable systems and show the results for maximum optomechanical-entanglement protection. In addition, we present a potential experimental implementation of this scheme. In Sec. IV, we extend these findings to an array of optical cavities with one oscillating end mirror, investigating the remote optimal optomechanical entanglement transmission for application purposes. Finally, in Sec. V, we summarize our findings and discuss the outlook for future research.

II. REFORMULATING DYNAMICS IN THE COHERENT-STATE REPRESENTATION

A. Construction of the Hamiltonian

We first construct an open-quantum-system description of a cavity optomechanical system in the coherent-state representation as shown in Fig. 1. The Fabry-Perot cavity, known as the simplest optical resonator structure, is additionally driven by a monochromatic laser, described by the radiation-pressure interaction between an optical cavity field and a vibrating end mirror, which applies to a wide variety of optomechanical devices, including microwave resonators [46], optomechanical crystals [47], and setups with a membrane inside a cavity [48].

Meanwhile, we assume that a cavity optomechanical system is coupled to two reservoirs. The optical mode is coupled to a reservoir characterized by zero-temperature electromagnetic modes, while the mechanical mode is coupled to another reservoir consisting of harmonic oscillators at thermal equilibrium [49]. In the Heisenberg picture, the system and environment evolve in time under the influence of the total Hamiltonian, which reads [50]

$$H_T = H_S + H_B, \quad (1)$$

where

$$\begin{aligned} H_S &= +\hbar\Delta_0 a^\dagger a + \hbar\omega_m b^\dagger b - \hbar\frac{G_0}{\sqrt{2}} a^\dagger a(b^\dagger + b) \\ &\quad + i\hbar(Ea^\dagger - E^*a), \end{aligned} \quad (2)$$

$$\begin{aligned} H_E &= +\hbar \sum_k \omega_k \Gamma_k^\dagger \Gamma_k + \hbar \sum_k g_k (\Gamma_k^\dagger a + a^\dagger \Gamma_k) \\ &\quad + \hbar \sum_n \omega_n \Lambda_n^\dagger \Lambda_n - i\hbar \sum_n \frac{\ell_n}{2} (\Lambda_n^\dagger - \Lambda_n)(b^\dagger + b), \end{aligned} \quad (3)$$

with a^\dagger (a) denoting b^\dagger (b) the creation (annihilation) operators of the optical mode and the mechanical mode, respectively. Laser detuning from the cavity resonance is $\Delta_0 = \omega_c - \omega_L$, where ω_c is the cavity characteristic frequency and ω_L is the driving laser frequency. The characteristic frequency and effective mass of the mechanical oscillator are ω_m and m , respectively. The optomechanical coupling coefficient is $G_0 = (\omega_c/L)\sqrt{\hbar/m\omega_m}$, with L being the cavity length. The complex amplitude of the driving laser is E . In addition, Γ_k^\dagger (Γ_k) and Λ_n^\dagger (Λ_n) for $k \in \{1, 2, 3, \dots, +\infty\}$ and $n \in \{1, 2, 3, \dots, +\infty\}$ are, respectively, the creation (annihilation) operators of the reservoirs for the optical mode and the mechanical mode. The harmonic-oscillator reservoirs have closely spaced frequencies corresponding to photons and phonons, denoted by ω_k and ω_n , respectively. The real numbers g_k and ℓ_n represent the coupling strengths between the subsystem and the n th reservoir mode, respectively. Details of the derivations of the total Hamiltonian (1) are attached in Appendix A [51].

B. Nonlinear Langevin equations

A reasonable description of the dynamics in an open quantum system should include photon losses in the optical cavity field and the Brownian noise acting on the vibrating end mirror. By substituting the total Hamiltonian (1) into the Heisenberg equation and taking into account the dissipation and noise terms, we obtain a set of closed integrodifferential equations (see Appendix B for the derivation [51]) for the operators of the optical mode and mechanical mode as follows:

$$\dot{q} = \omega_m p, \quad (4)$$

$$\dot{p} = -\omega_m q - \gamma_m p + G_0 a^\dagger a + \xi, \quad (5)$$

$$\dot{a} = -(\kappa + i\Delta_0)a + iG_0 aq + E + \sqrt{2\kappa} a_{\text{in}}, \quad (6)$$

where $q = (b^\dagger + b)/\sqrt{2}$ and $p = i(b^\dagger - b)/\sqrt{2}$ are the dimensionless position and momentum operators of the

vibrating end mirror. We assume that the decay rate of the optical cavity is κ and set the mechanical damping rate as $\gamma_m = \omega_m \gamma$. The dissipative terms κ and γ are proportional to the square of the coupling strength between the subsystem and the reservoir g_k and ℓ_n , respectively. The optical Langevin force a_{in} represents the field incident to the cavity and is assumed to be in the vacuum state. Its specific expression and the correlation function [52] are

$$\begin{aligned} a_{\text{in}}(t) &= \frac{-i}{\sqrt{2\pi}} \sum_k g_k \Gamma(t_0) e^{-i\omega_k(t-t_0)}, \\ \langle a_{\text{in}}(t) a_{\text{in}}^\dagger(t') \rangle &= \delta(t - t'), \end{aligned} \quad (7)$$

where t_0 represents the initial time. This correlation function is true for optical fields at room temperature or microwaves at a cryostat.

In contrast, the Brownian noise operator is given by

$$\xi(t) = \sum_n \frac{i\ell_n}{\sqrt{2}} [\Lambda_n^\dagger(t_0) e^{i\omega_n(t-t_0)} - \Lambda_n(t_0) e^{-i\omega_n(t-t_0)}]. \quad (8)$$

The mechanical damping force ξ is non-Markovian in general [53], but it can be treated as Markovian if the following two conditions are met: the thermal bath occupation number satisfies $\bar{n} \gg 1$; and the mechanical quality factor satisfies $Q = \omega_m/\gamma_m = 1/\gamma \gg 1$. These conditions are well satisfied in the majority of contemporary experimental setups, which validates the use of the standard Markovian delta-correlation [54,55]:

$$\frac{\langle \xi(t) \xi(t') + \xi(t') \xi(t) \rangle}{2} \approx \gamma_m (2\bar{n} + 1) \delta(t - t'), \quad (9)$$

where $\bar{n} = [\exp(\hbar\omega_m/k_B T) - 1]^{-1}$ is the mean thermal excitation number with the Boltzmann constant k_B and the end-mirror temperature T .

So far, we have constructed the total Hamiltonian of the optomechanical system under the coherent-state representation and completely reproduced the results of the nonlinear Langevin equations in Ref. [28], which provides solid support for the filtering model dominated by the resonance effect discussed later. We stress that deriving the Langevin equation from the total Hamiltonian provides a clear picture in explicitly revealing the specific form of the interaction between the system and the environment and the physical origin of each term in the nonlinear Langevin equations, in comparison to the implicit treatment of such interactions in the Lindblad master equation.

III. RESONANCE-DOMINANT OPTOMECHANICAL ENTANGLEMENT

A. Filtering model

In the preceding section, the total Hamiltonian (1) describes an original interaction between an optomechanical system and its surrounding environment. This section

proposes a resonant filtering model in the weak-coupling limit between the system and the heat bath. It uses a high-frequency resonance between the mechanical mode and its thermal reservoirs to filter out nonresonant degrees of freedom and achieve quantum coherence protection.

To discuss the frequency relation between the mechanical mode and its thermal reservoirs, we introduce the frequency transformation $\tilde{b}(t) = b(t) \exp(i\omega_m t)$ and $\tilde{\Lambda}_n(t) = \Lambda_n(t) \exp(i\omega_n t)$ for $b(t)$ and $\Lambda_n(t)$ [49] in the interaction picture. After that, the Hamiltonian (1) reads

$$\begin{aligned} H_T = & +\hbar\Delta_0 a^\dagger a + \hbar\omega_m b^\dagger b + i\hbar(Ea^\dagger - E^*a) \\ & - \hbar \frac{G_0}{\sqrt{2}} a^\dagger a (\tilde{b}^\dagger e^{i\omega_m t} + \tilde{b} e^{-i\omega_m t}) + \hbar \sum_k \omega_k \Gamma_k^\dagger \Gamma_k \\ & + \hbar \sum_k g_k (\Gamma_k^\dagger a + a^\dagger \Gamma_k) + \hbar \sum_n \omega_n \Lambda_n^\dagger \Lambda_n \\ & - i\hbar \sum_n \frac{\ell_n}{2} [\tilde{\Lambda}_n^\dagger \tilde{b} e^{i(\omega_n - \omega_m)t} - \tilde{b}^\dagger \tilde{\Lambda}_n e^{-i(\omega_n - \omega_m)t}] \\ & - i\hbar \sum_n \frac{\ell_n}{2} [\tilde{\Lambda}_n^\dagger \tilde{b}^\dagger e^{i(\omega_n + \omega_m)t} - \tilde{b} \tilde{\Lambda}_n e^{-i(\omega_n + \omega_m)t}]. \end{aligned} \quad (10)$$

As mentioned above, our physical model describes a Markovian process in the weak-coupling limit $\gamma \ll 1$, which corresponds to Eq. (10) satisfying the weak-coupling limit $\ell_n \ll 1$ for $n \in \{1, 2, 3, \dots, +\infty\}$ [56]. See Fig. 2 for a schematic diagram of the filtering model. We eliminate the relatively fast-oscillating terms from Eq. (10) and then perform the inverse frequency transformation as $b(t) = \tilde{b}(t) \exp(-i\omega_m t)$ and $\Lambda_n(t) = \tilde{\Lambda}_n(t) \exp(-i\omega_n t)$. Through this process, we classify the filtering model reduced from Eq. (10) into the following two cases.

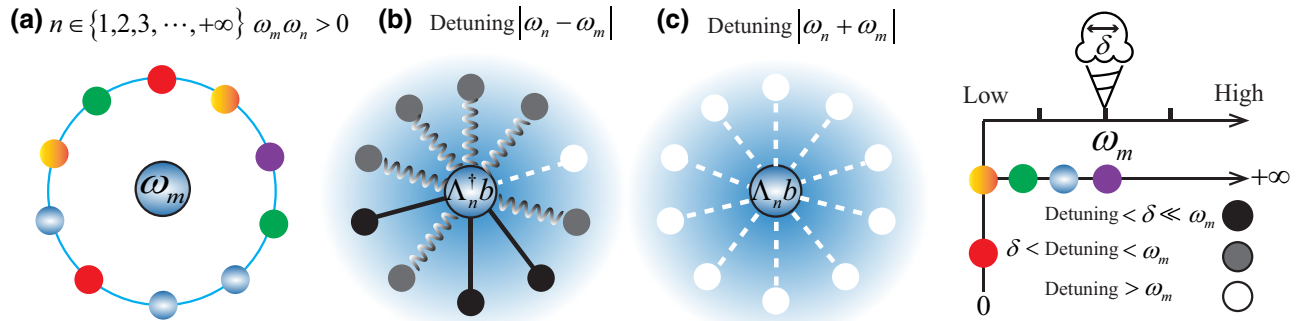


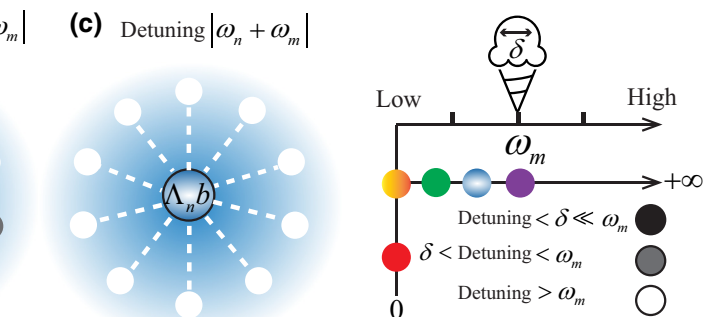
FIG. 2. Schematic diagram of the filtering model. (a) The coupling between a high-frequency mechanical oscillator and codirectional thermal reservoirs. The frequency of the thermal reservoirs sequentially transits from zero to positive infinity in rainbow color order. (b) The terms $\tilde{\Lambda}_n^\dagger \tilde{b}$ and $\tilde{b}^\dagger \tilde{\Lambda}_n$ show the high-frequency resonance effect. (c) The terms $\tilde{\Lambda}_n^\dagger \tilde{b}^\dagger$ and $\tilde{b} \tilde{\Lambda}_n$ exhibit large detuning effects. The black, gray, and white colors correspond to the high-frequency resonance, moderately detuned, and highly detuned modes of the heat bath compared to the frequency of the single-mode mechanical oscillator ω_m . The parameters δ and ω_m can be modulated by coherent laser driving [57,58].

The high-frequency resonance region commonly exists in the coupling between the mechanical mode and the heat bath composed of positive energy modes denoted as $\omega_m \omega_n > 0$ and $\omega_n \in (0, +\infty)$. The high-frequency resonance results in level repulsion between ω_m and ω_n [59]. Here we propose to filter out the strongly nonresonant contributions $\tilde{\Lambda}_n^\dagger \tilde{b}^\dagger$ and $\tilde{b} \tilde{\Lambda}_n$ mechanically; see Sec. III D for possible experimental realizations. Keeping only the resonant terms $\tilde{\Lambda}_n^\dagger \tilde{b}$ and $\tilde{b}^\dagger \tilde{\Lambda}_n$, the filtering model is $H_F = H_T + i\hbar \sum_n \ell_n (\Lambda_n^\dagger b^\dagger - \Lambda_n b)/2$. The resonance terms $\tilde{\Lambda}_n^\dagger \tilde{b}$ and $\tilde{b}^\dagger \tilde{\Lambda}_n$ in this region describe the exchange of quanta between the mechanical mode and its n th thermal reservoir mode [18].

In contrast, the high-frequency inverse-resonance region occurs in the coupling between the mechanical mode and the unstable heat bath composed of negative energy modes, denoted as $\omega_m \omega_n < 0$ and $\omega_n \in (-\infty, 0)$. The high-frequency inverse resonance results in level attraction between ω_m and ω_n ; details can be found in Appendix C [60]. Keeping only the terms of $\tilde{\Lambda}_n^\dagger \tilde{b}^\dagger$ and $\tilde{b} \tilde{\Lambda}_n$, the inverse-filtering model reads $H_F^I = H_T + i\hbar \sum_n \ell_n (\Lambda_n^\dagger b - b^\dagger \Lambda_n)/2$. The inverse-resonance terms $\tilde{\Lambda}_n^\dagger \tilde{b}^\dagger$ and $\tilde{b} \tilde{\Lambda}_n$ in this region represent a two-mode squeezing interaction between the mechanical mode and its n th thermal reservoir mode, and the parametric amplification relies on the two-mode squeezing interaction [61]. In the following, we focus on discussing the high-frequency resonance range since its physical significance is clear and universal.

B. The Lyapunov equation for the steady-state correlation matrix

In order to comprehend the impact of resonance effects between a mechanical mode and its thermal reservoirs on the strength of an optomechanical system, it



is crucial to gain insight into the structure of optomechanical correlation in open quantum systems. For this purpose, we use the Lyapunov equation to compute the steady-state correlation matrix between subsystems and obtain the optomechanical entanglement strength [62]. Without loss of generality, we take the high-frequency resonance regime as an example of deriving the Lyapunov equation in terms of the steady-state correlation matrix.

By deriving the Heisenberg equation of motion of the resonant Hamiltonian H_F , we obtain nonlinear Langevin equations that govern the dynamical behavior of the optomechanical system in the high-frequency resonance regime. The nonlinear Langevin equations are written as (see Appendix D for details)

$$\dot{q} = \omega_m p + \frac{\gamma}{4} \dot{p} + \frac{1}{2} \xi', \quad (11)$$

$$\dot{p} = -\omega_m q - \frac{\gamma}{4} \dot{q} + G_0 a^\dagger a + \frac{1}{2} \xi, \quad (12)$$

$$\dot{a} = -(\kappa + i\Delta_0)a + iG_0 aq + E + \sqrt{2\kappa} a_{\text{in}}, \quad (13)$$

where the Brownian noise operator reads

$$\xi'(t) = \sum_n \frac{\ell_n}{\sqrt{2}} [\Lambda_n^\dagger(t_0) e^{i\omega_n(t-t_0)} + \Lambda_n(t_0) e^{-i\omega_n(t-t_0)}], \quad (14)$$

which has the same delta-correlated form as $\xi(t)$ under the weak-coupling limit $\gamma \ll 1$.

The nonlinear Langevin equations (11)–(13) are inherently nonlinear as they contain a product of the photon operator and dimensionless position operator of the mechanical phonon, aq , as well as a quadratic term in photon operators, $a^\dagger a$. Using the standard mean-field method [63] to solve Eqs. (11)–(13), we start by splitting each Heisenberg operator into the classical mean values and quantum fluctuation operators, i.e., $a = \alpha_s + \delta a$ as in $a^\dagger = \alpha_s^* + \delta a^\dagger$, $q = q_s + \delta q$, and $p = p_s + \delta p$, thereby linearizing these equations. Adopting the above approach and inserting these expressions into the nonlinear Langevin equations (11)–(13), we find the solution of the mean values for the classical steady state given by $p_s = 0$, $q_s = G_0 \alpha_s^* \alpha_s / \omega_m$, and $\alpha_s = E / (\kappa + i\Delta)$, where we set the normalization of the detuning frequency of the optical field as $\Delta = \Delta_0 - G_0^2 \alpha_s^* \alpha_s / \omega_m$.

The parameter regime for generating optomechanical entanglement is the one with a large amplitude of the driving laser E , i.e., $\alpha_s \gg \delta a$ and $\alpha_s^* \gg \delta a^\dagger$. By dropping the contribution from the second-order small terms, as described in Appendix E, we obtain the linearized Langevin equations

$$\delta \dot{q} = \omega_m \delta p - \frac{\gamma_m}{4} \delta q + \frac{1}{2} \xi', \quad (15)$$

$$\delta \dot{p} = -\omega_m \delta q - \frac{\gamma_m}{4} \delta p + G_0 (\alpha_s^* \delta a + \alpha_s \delta a^\dagger) + \frac{1}{2} \xi, \quad (16)$$

$$\delta \dot{a} = -(\kappa + i\Delta) \delta a + iG_0 \alpha_s \delta q + \sqrt{2\kappa} a_{\text{in}}. \quad (17)$$

By assuming the driving laser amplitude $E = |E| \exp(i\varphi)$, where $|E|$ is related to the input laser power P by $|E| = \sqrt{2P\kappa/\hbar\omega_L}$ and φ denotes the phase of the laser field coupling to the optical cavity field, we choose φ to satisfy $\tan(\varphi) = \Delta/\kappa$ so that α_s may be real.

The quadratures play an essential role in studying entanglement because they are used to quantify the correlations between different modes. We define the cavity field quadratures $\delta X = (\delta a + \delta a^\dagger)/\sqrt{2}$ and $\delta Y = i(\delta a^\dagger - \delta a)/\sqrt{2}$ as two observables that describe the quantum state of a cavity field mode, which can be measured using homodyne detection techniques.

Accordingly, we define the orthogonal input noise operators $X_{\text{in}} = (\delta a_{\text{in}}^\dagger + \delta a_{\text{in}})/\sqrt{2}$ and $Y_{\text{in}} = i(\delta a_{\text{in}}^\dagger - \delta a_{\text{in}})/\sqrt{2}$, and thereby Eqs. (15)–(17) can be written in matrix form as

$$\dot{\mu}(t) = A\mu(t) + n(t). \quad (18)$$

Here the components of each matrix are as follows: the transposes of the column vector of continuous-variable fluctuation operators are written as $\mu^T(t) = [\delta q(t), \delta p(t), \delta X(t), \delta Y(t)]$; the transposes of the column vector of noise operators are denoted by $n^T(t) = [0.5\xi'(t), 0.5\xi(t), \sqrt{2\kappa}X_{\text{in}}(t), \sqrt{2\kappa}Y_{\text{in}}(t)]$; and the coefficient matrix A in terms of system parameters takes the form

$$A = \begin{pmatrix} -0.25\gamma_m & \omega_m & 0 & 0 \\ -\omega_m & -0.25\gamma_m & G & 0 \\ 0 & 0 & -\kappa & \Delta \\ G & 0 & -\Delta & -\kappa \end{pmatrix}, \quad (19)$$

where the effective optomechanical coupling is given by $G = \sqrt{2\alpha_s}G_0$.

The solution of Eq. (18) can be expressed as

$$\mu(t) = M(t)\mu(t_0) + \int_{t_0}^t M(\tau)n(t-\tau)d\tau, \quad (20)$$

where M is the matrix exponential $M(t) = \exp(At)$ and we assume the initial time as $t_0 = 0$. The system is stable if and only if the real parts of all the eigenvalues of the matrix A are negative. The eigenvalue equation $\det[A - \lambda I_4] = [(0.25\gamma_m + \lambda)^2 + \omega_m^2][(k + \lambda)^2 + \Delta^2] - \omega_m G^2 \Delta = 0$, where I_4 denotes the four-dimensional identity matrix, can be reduced to the fourth-order equation $C_0\lambda^4 + C_1\lambda^3 + C_2\lambda^2 + C_3\lambda + C_4 = 0$. The stability conditions can be derived by applying the Routh-Hurwitz criterion [64] as follows: $C_0 > 0$, $C_1 > 0$, $C_1 C_2 - C_0 C_3 > 0$, $(C_1 C_2 - C_0 C_3)C_3 - C_1^2 C_4 > 0$, and $C_4 > 0$, yielding the

following two nontrivial conditions: $(\omega_m^2 + \gamma_m^2/16)(\Delta^2 + \kappa^2) - \omega_m G^2 \Delta > 0$ and

$$\begin{aligned} &+ \gamma_m \kappa \left\{ \Delta^4 + \Delta^2 \left(\frac{\gamma_m^2}{8} + \gamma_m \kappa + 2\kappa^2 - 2\omega_m^2 \right) \right. \\ &\quad \left. + \frac{1}{256} [16\omega_m^2 + (\gamma_m + 4\kappa)^2]^2 \right\} \\ &+ \omega_m G^2 \Delta \left(\frac{\gamma_m}{2} + 2\kappa \right)^2 > 0. \end{aligned} \quad (21)$$

The following numerical simulation shows that realistic experimental parameter configurations always meet these stability conditions. When the system is stable, it reaches a unique steady state in the long-time limit $t \rightarrow +\infty$ independently of the initial condition.

We set the initial condition to a Gaussian state, and the linear dynamics preserves the noise operators ξ' , ξ , and a_{in} . Thus, the correlation properties of the system can be completely characterized by its two first moments, of which we are interested in the second one, namely the covariance matrix with elements defined as

$$\begin{aligned} V_{ij} &= \frac{1}{2} \langle \mu_i(+\infty) \mu_j(+\infty) + \mu_j(+\infty) \mu_i(+\infty) \rangle \\ &= \sum_{k,l} \int_{t_0}^{+\infty} d\tau \int_{t_0}^{+\infty} d\tau' M_{ik}(\tau) M_{jl}(\tau') \Phi_{kl}(\tau - \tau'), \end{aligned} \quad (22)$$

where $\Phi_{kl}(\tau - \tau') = \langle n_k(\tau) n_l(\tau') + n_l(\tau') n_k(\tau) \rangle / 2$ is the matrix of the stationary noise correlation functions. Because the matrix elements are independent of $n(t)$, we obtain $\Phi_{kl}(\tau - \tau') = D_{kl} \delta(\tau - \tau')$, where $D = \text{diag}[\gamma_m(2\bar{n} + 1)/4, \gamma_m(2\bar{n} + 1)/4, \kappa, \kappa]$ is a diagonal matrix. According to Eq. (22) and the form of $\Phi_{kl}(\tau - \tau')$, we find that the expression of the matrix V is equivalent to

$$V = \int_{t_0}^{+\infty} M(\tau) D M(\tau)^T d\tau, \quad (23)$$

which leads to a linear Lyapunov equation with respect to V , i.e., $A V + V A^T = -D$. See Appendix F for a detailed derivation of the Lyapunov equation.

In addition, we can derive a Lyapunov equation satisfied by the high-frequency inverse-resonance Hamiltonian H_F^I similarly to the form of the high-frequency resonance Hamiltonian H_F . Moreover, we show that the analysis and results concerning optomechanical entanglement in the high-frequency inverse-resonance regime are equivalent to those in the high-frequency resonance regime. Therefore, we do not elaborate on it further here.

C. Optomechanical entanglement

Cavity optomechanical systems naturally exhibit complex entanglement structures and always involve mixed states and continuous-variable entanglement, which are affected by dissipation and noise. In this sense, logarithmic negativity is a powerful tool that can provide valuable insights into the nature of optomechanical entanglement [65], which can be experimentally measured using homodyne detection. Thus, we use logarithmic negativity E_N to measure optomechanical entanglement between the optical cavity field and the mechanical oscillator. It provides an obvious easy way to compute an upper bound for the distillable optomechanical entanglement [30].

As mentioned in the continuous-variable scenario, the bipartite optomechanical entanglement can be quantified as [62]

$$E_N = \max [0, -\ln(2\Xi)], \quad (24)$$

where

$$\Xi = \frac{1}{\sqrt{2}} \left\{ \Sigma(V) - \sqrt{[\Sigma(V)]^2 - 4 \det(V)} \right\}^{1/2} \quad (25)$$

is the lowest symplectic eigenvalue of the partial transpose of the 4×4 steady-state correlation matrix [66]. For simplicity, we denote the 4×4 steady-state correlation matrix in 2×2 block matrix form, which is given by $V = [(\Theta, \beta), (\beta^T, \eta)]$ and $\Sigma(V) = \det(\Theta) + \det(\eta) - 2 \det(\beta)$. We note that a Gaussian state is entangled if and only if $\Xi < 1/2$. This is equivalent to Simon's entanglement criterion for all bipartite Gaussian states [67], which can be written as $4 \det(V) < \Sigma(V) - 1/4$.

We numerically calculated the negativity for cavity optomechanical systems as shown in Figs. 3 and 4. In our numerical simulation, we utilize parameter values identical to those outlined in Ref. [28], which agree with the current optomechanical experimental configurations [68–71] and satisfy the stability conditions (21). To begin with, we set the initial closed optomechanical system in a maximum optomechanical entangled state. For simplicity, we assume that the driving laser frequency ω_L is resonant with the characteristic frequency ω_c of the cavity field, that is, the laser detuning from the cavity resonance satisfies $\Delta_0 = 0$.

In Fig. 3, we compare the sensitivity of the optomechanical entanglement E_N to the mechanical damping rate γ_m for the two optomechanical systems, H_T and H_F . We show a significant enhancement of the robustness of optomechanical entanglement for H_F against γ_m . Specifically, we observe that the length of the black downward-pointing arrow in Fig. 3(b) is approximately half of that in Fig. 3(a), which implies that the optomechanical entanglement of the filtering model H_F is almost twice as robust to γ_m as the original model H_T . Additionally, it is worth noting that the presence of optomechanical entanglement is only within

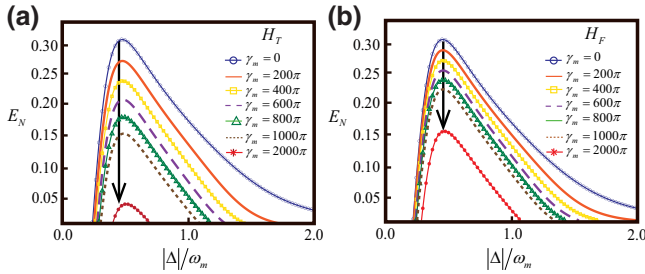


FIG. 3. Plot of the logarithmic negativity E_N as a function of the normalized detuning frequency of the optical field $|\Delta|$ (in units of ω_m) for seven values of the mechanical damping rate: $\gamma_m = 0$ (blue circle line), $\gamma_m = 200\pi$ Hz (orange solid line), $\gamma_m = 400\pi$ Hz (yellow square line), $\gamma_m = 600\pi$ Hz (purple dashed line), $\gamma_m = 800\pi$ Hz (green triangle line), $\gamma_m = 1000\pi$ Hz (brown dotted line), and $\gamma_m = 2000\pi$ Hz (red symbol line), where (a) and (b) correspond to the original model H_T and the filtering model H_F , respectively. The length of the black downward-pointing arrows indicates how sensitive optomechanical entanglement is to γ_m . The other parameters for both panels are chosen as follows: optical cavity of length $L = 1$ mm and driving laser with wavelength $\lambda = 810$ nm and power $P = 50$ mW. The decay rate of the optical cavity is chosen to be $\kappa = 8.8\pi \times 10^6$ Hz, the optical finesse $F = \pi c/L\kappa \approx 3.4 \times 10^4$ with $c = 3 \times 10^8$ m/s, and the driving laser frequency is resonant with the characteristic frequency of the cavity field, $\omega_L = \omega_c = 2\pi c/\lambda$. The mechanical oscillator has the characteristic frequency $\omega_m = 20\pi$ MHz, the effective mass $m = 50$ ng, and its temperature is $T = 400$ mK [28].

a limited range of $|\Delta|$ around $|\Delta| \approx \omega_m$, which means that the frequency resonance between the normalization of the detuning frequency of the optical field $|\Delta|$ and the frequency of the mechanical oscillator ω_m plays a dominant role in the generation of optomechanical entanglement.

We further examine the impact of the resonance effect between the mechanical mode and its thermal reservoir on the properties of optomechanical entanglement. For this purpose, we set $\gamma_m = 200\pi$ Hz according to the actual laboratory conditions.

Figure 4(a) shows the logarithmic negativity E_N versus the normalized detuning frequency of the optical field $|\Delta|$ (in units of ω_m) for model cases: high-frequency resonance of the filtering model H_F , high-frequency inverse resonance of the filtering model H_F^I , and original system H_T . It shows that the maximum optomechanical entanglements for H_F and H_F^I are equal to each other, while that for H_T is less. The results indicate that the resonance effect can safeguard the maximum optomechanical entanglement by filtering out the contributions from a largely detuned part of the degree of freedom, ultimately reducing both the Brownian noise ξ (ξ') and the mechanical dissipation γ_m .

The robustness of such an entanglement E_N with respect to the environmental temperature T of the mirror is shown

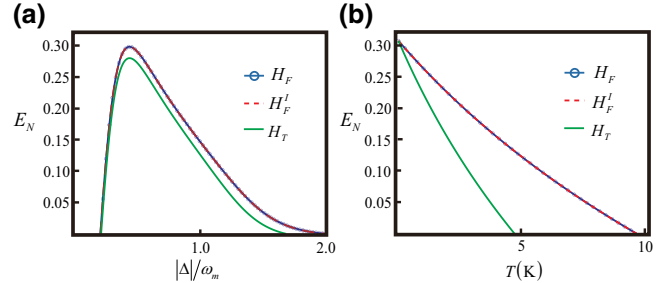


FIG. 4. Comparison of the optomechanical-entanglement properties under different mechanisms: high-frequency resonance of the filtering model H_F (blue circle line), high-frequency inverse resonance of the filtering model H_F^I (red dashed line), and original model H_T (green solid line). (a) Plot of the logarithmic negativity E_N as a function of the normalized detuning frequency of the optical field $|\Delta|$ (in units of ω_m). We set $\gamma_m = 200\pi$ Hz and $T = 400$ mK. (b) Plot of the logarithmic negativity E_N versus the mirror temperature T . We set $\gamma_m = 200\pi$ Hz and $\Delta = 0.5\omega_m = 10\pi$ MHz. In both panels, the other parameter values are the same as in Fig. 3.

in Fig. 4(b). We find that the optomechanical entanglement of the filtering model H_F remains even at temperatures around 10 K and is twice the magnitude of the persistent temperature in the original model H_T . In addition, we observe that the high-frequency resonance and the high-frequency inverse-resonance regimes have completely equivalent effects on optomechanical entanglement.

In summary, we have discussed the impact of the high-frequency resonance effect between the mechanical oscillator and its thermal reservoir on optomechanical entanglement. We have found that the resonance effect doubles the robustness of optomechanical entanglement to mechanical dissipation and the mirror temperature. We have achieved the maximum protection of optomechanical entanglement by constructing a filtering model using resonance effects. We have observed numerically that both the high-frequency resonance and the high-frequency inverse-resonance regimes have equivalent effects on optomechanical entanglement.

D. Experimental implementation

We propose materializing the present theoretical filtering model in resistor-inductor-capacitor circuit [72–74] or superconducting quantum interference device experiments [75]. Here, we focus on the high-frequency resonance region. As shown in Fig. 5, we build an oscillatory circuit consisting of a capacitor C , an inductor L , a thermistor R_T , and an oscillator X . We set the normalized detuning frequency of the optical field of the LC circuit to satisfy $|\Delta| = 1/(2\pi\sqrt{LC}) = 20\pi$ MHz.

First, the mechanical resonator (blue) and the optical cavity (green) are connected via an inductor. Second, an

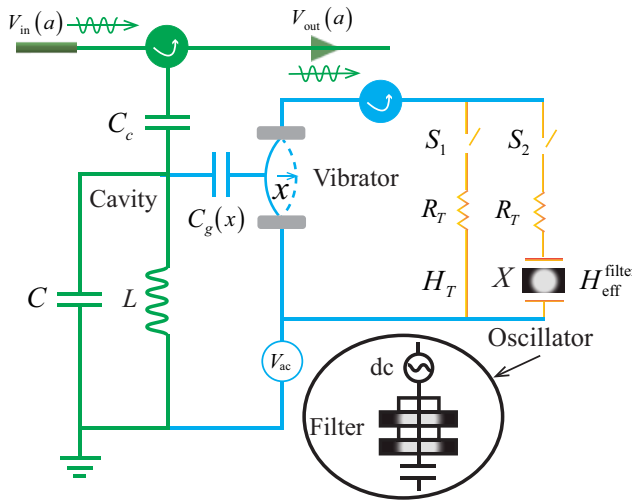


FIG. 5. A circuit consisting of a resistor, inductor, and capacitor can be used to build an oscillatory filtering model for high-frequency resonance. This experimental setup comprises an on-chip optical cavity (green) coupled with a high-quality-factor nanomechanical resonator. By turning on switch S_1 and turning off switch S_2 , the thermistor (orange) will provide a thermal environment that couples with the resonator, corresponding to the original model H_T . Conversely, the thermistor and the oscillator (black) will generate a high-frequency oscillation thermal environment that couples with the resonator, corresponding to the filtering model H_F . Direct current (dc) is used for signal frequency readout.

extensive ac voltage bias V_{ac} is applied in order to excite the mechanical resonator, represented as a movable capacitance $C_g(x)$. To obtain the maximum optomechanical entanglement, the frequency of the applied voltage should be close to $|\Delta|$, namely $|\Delta| \approx \omega_m$. Next, as the LC circuit oscillates, a current is induced in the thermistor, generating a temperature change due to the Joule heating effect. Therefore, by turning on switch S_1 and turning off switch S_2 simultaneously, the mechanical resonator will be coupled to a full-frequency thermal reservoir, corresponding to the original model H_T . In contrast, the largely detuned part of the degree of freedom can be filtered by applying the oscillator X if we turn off S_1 while turning on S_2 . The oscillator X is an electronic circuit component capable of generating a specific frequency signal and can be utilized as a filter to filter out unwanted frequency components selectively. Specifically, when the input signal matches the resonant frequency of the oscillator, it amplifies the input signal and outputs a near-resonant signal, thereby achieving high-frequency oscillatory wave filtering. Thus, the resistor-inductor-capacitor oscillatory circuit can be described by the filtering model H_F .

In addition, we need to choose a mechanical resonator with a giant mechanical quality factor to ensure that significant quantum effects are achievable, that is, $Q = \omega_m/\gamma_m = 1/\gamma \gg 1$ corresponding to the weak-coupling

limit $\gamma \ll 1$. The remaining parameter values for the simulation of the circuit experiment are the same as in Fig. 4(a). Furthermore, we note that, with optical interferometry techniques [76,77], we can observe the resonance response of a mechanical resonator to its thermal environment. Homodyne detection techniques [78,79] can be used to measure an optomechanical entanglement.

It is important to note that experimental studies on open-system dynamics with linear optical setups often use approximated simulations of quantum channels, such as amplitude decay or phase-damping channels [80–83]. These simulations rely on the rotating-wave approximation for system-bath interactions and the weak-coupling approximation. Recently, we noted that a study that aims to test the difference between the rotating-wave approximation and non-rotating-wave approximation channels by studying the varying dynamics of quantum temporal steering was demonstrated experimentally [84,85].

IV. GENERALIZED EXTENSION AND APPLICATION

We are now extending the theory of resonance-dominant entanglement to a multimode optomechanical system. Specifically, we discuss an optical-cavity array with one oscillating end mirror and investigate optimal optomechanical-entanglement transmission.

As schematically shown in Fig. 6, the system comprises an oscillating end mirror coupled to an array of optical cavities. The adjacent optical cavities are linearly coupled with an interaction strength of J [86]. A laser field drives the left end of the optical cavity, while the right end is connected to a vibrating end mirror.

If we consider this system satisfying the resonance regime, the total Hamiltonian of this open quantum system can be written as

$$\begin{aligned} H = & +\hbar\Delta_0 a_1^\dagger a_1 + \sum_{j=2}^N \omega_{c_j} a_j^\dagger a_j + \hbar\omega_m b^\dagger b \\ & + i\hbar \left(E a_1^\dagger - E^* a_1 \right) + \hbar \sum_{j=1}^{N-1} J \left(a_j^\dagger a_{j+1} + a_{j+1}^\dagger a_j \right) \\ & - \hbar \frac{G_0}{\sqrt{2}} a_N^\dagger a_N (b^\dagger + b) + \hbar \sum_{j=1}^N \sum_k \omega_{jk} \Gamma_{jk}^\dagger \Gamma_{jk} \end{aligned}$$

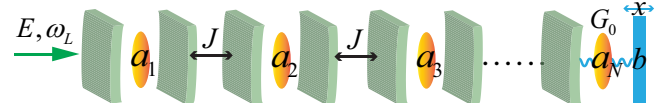


FIG. 6. Schematic diagram depicting a one-dimensional array of optical cavities coupled via linear hopping between each cavity, with an oscillating end mirror.

$$+ \hbar \sum_{j=1}^N \sum_k g_{jk} (\Gamma_{jk}^\dagger a_j + a_j^\dagger \Gamma_{jk}) \\ + \hbar \sum_n \omega_n \Lambda_n^\dagger \Lambda_n - i\hbar \sum_n \frac{\ell_n}{2} (\Lambda_n^\dagger b - b^\dagger \Lambda_n), \quad (26)$$

where a_j^\dagger (a_j) and Γ_{jk}^\dagger (Γ_{jk}) are the corresponding creation (annihilation) operators for the j th optical cavity mode and its thermal reservoir modes with frequencies ω_{cj} and ω_{jk} , respectively, and the coupling strength between them is g_{jk} .

Similarly, the nonlinear Langevin equations for the operators of the mechanical and optical modes are given as follows:

$$\dot{q} = \omega_m p - \frac{\gamma_m}{4} q + \frac{1}{2} \xi', \\ \dot{p} = -\omega_m q - \frac{\gamma_m}{4} p + G_0 a_N^\dagger a_N + \frac{1}{2} \xi, \\ \dot{a}_1 = -(\kappa + i\Delta_0) a_1 - iJ a_2 + E + \sqrt{2\kappa} a_1^{\text{in}}, \\ \vdots \\ \dot{a}_j = -(\kappa + i\omega_{cj}) a_j - iJ (a_{j-1} + a_{j+1}) + \sqrt{2\kappa} a_j^{\text{in}}, \\ \vdots \\ \dot{a}_N = -(\kappa + i\omega_{cN}) a_N - iJ a_{N-1} + iG_0 q a_N + \sqrt{2\kappa} a_N^{\text{in}}, \quad (27)$$

where we assume that all optical-cavity fields share the same coupling strength, $g_{jk} = g_k$, i.e., $\kappa_j = \kappa$. As the simplest case, we consider $N = 2$ to study the optomechanical entanglement properties of this system. Similarly, we use the logarithmic negativity to measure the entanglement between two arbitrary bosonic modes in the system. Now, we focus on the numerical evaluation of the bipartite entanglement E_N^{mc-1} to show the optimal remote optomechanical-entanglement transfer.

In the two-cavity case, we let E_N^{mc-1} , E_N^{mc-2} , and E_N^{cc-12} denote the logarithmic negativity between the mirror and cavity 1, the mirror and cavity 2, and cavity 1 and cavity 2, respectively. In Fig. 7(a), we plot E_N^{mc-1} , E_N^{mc-2} , and E_N^{cc-12} as functions of the normalized detuning $|\varpi|$ (in units of ω_m) with the other parameters set to $\Delta_0 = 0$, $J = 0.7\omega_m$, and $T = 400$ mK. The normalized detuning $\varpi = \omega_{c2} - G_0 Q_s$ depends on the steady-state mean values $Q_s = G_0 \alpha_{2s}^* \alpha_{2s} / \omega_m$, and $\alpha_{2s} = -iJ \alpha_{1s} / (\kappa + i\varpi)$ with $\alpha_{1s} = E / [\kappa + i\Delta_0 + J^2 / (\kappa + i\varpi)]$, which can be obtained by setting the time derivative to zero in the nonlinear Langevin equation (27) for $N = 2$. Our numerical findings show that by tuning the magnitude of ϖ , we are able to achieve long-distance optomechanical-entanglement transfer. As $|\varpi|$ increases approximately from $0.50\omega_m$ to $0.65\omega_m$, the distant optomechanical entanglement E_N^{mc-1} correspondingly increases at the expense

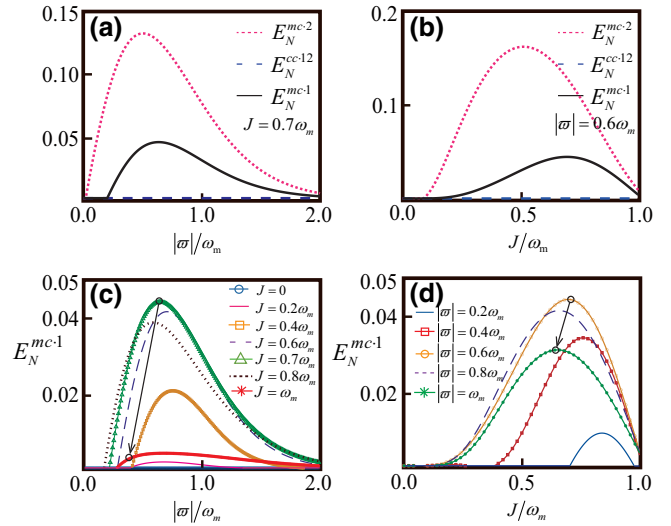


FIG. 7. The optimal remote optomechanical-entanglement transmittance. (a) The negativity entanglements E_N^{mc-1} (pink dotted line), E_N^{mc-2} (black solid line), and E_N^{cc-12} (blue dashed line) as functions of the normalized detuning $|\varpi|$ (in units of ω_m) with the other parameters set to $\Delta_0 = 0$ and $J = 0.7\omega_m$. (b) The negativity entanglements E_N^{mc-1} , E_N^{mc-2} , and E_N^{cc-12} versus the linear hopping strength J (in units of ω_m) with the other parameters set to $\Delta_0 = 0$ and $|\varpi| = 0.6\omega_m$. (c) The negativity entanglements E_N^{mc-1} as a function of $|\varpi|$ (in units of ω_m) for different values of the linear hopping rate: $J = 0$ (blue circle line), $J = 0.2\omega_m$ (pink solid line), $J = 0.4\omega_m$ (orange square line), $J = 0.6\omega_m$ (purple dashed line), $J = 0.7\omega_m$ (green triangle line), $J = 0.8\omega_m$ (brown dotted line), and $J = \omega_m$ (red symbol line). (d) The negativity entanglements E_N^{mc-1} as a function of J (in units of ω_m) for different values of the normalized detuning: $|\varpi| = 0.2\omega_m$ (blue solid line), $|\varpi| = 0.4\omega_m$ (red square line), $|\varpi| = 0.6\omega_m$ (orange circle line), $|\varpi| = 0.8\omega_m$ (purple dashed line), and $|\varpi| = \omega_m$ (green symbol line). The remaining parameter values for all panels are set to be the same as in Fig. 4.

of the decrease of the neighboring optomechanical entanglement E_N^{mc-2} , due to the adjacent cavities acting as entanglement transmitters.

In Fig. 7(b), we plot E_N^{mc-1} , E_N^{mc-2} , and E_N^{cc-12} as functions of the linear hopping strength J (in units of ω_m) with the other parameters set to $\Delta_0 = 0$, $|\varpi| = 0.6\omega_m$, and $T = 400$ mK. In a similar analysis, we can also implement distant optomechanical-entanglement transfer by adjusting the strength of J approximately from $0.5\omega_m$ to $0.75\omega_m$. In particular, when $T = 400$ mK, we find that the optimal remote optomechanical-entanglement transfer occurs around $|\varpi| = 0.6$ and $J = 0.7$ (in units of ω_m), and the maximum value of remote entanglement E_N^{mc-1} is approximately evaluated at 0.045; see Figs. 7(c) and 7(d).

V. SUMMARY AND PROSPECT

In summary, we have demonstrated that resonance effects between a mechanical mode and its thermal

environment can protect optomechanical entanglement. Specifically, we have shown that resonance effects nearly double the robustness of the optomechanical entanglement against mechanical dissipation and its environmental temperature. The mechanism of optomechanical-entanglement protection involves the elimination of degrees of freedom associated with significant detuning between the mechanical mode and its thermal reservoirs, thereby counteracting the decoherence. We have revealed that this approach is particularly effective when both near-resonant and weak-coupling conditions are simultaneously satisfied between a mechanical mode and its environment. We have also proposed a feasible experimental implementation for the filtering model to observe these phenomena. Furthermore, we extended this theory to an optical cavity array with one oscillating end mirror and investigated optimal optomechanical-entanglement transfer. This study represents a significant advancement in the application of resonance effects for protecting quantum systems against decoherence, thereby opening up new possibilities for large-scale quantum information processing and the construction of quantum networks.

In addition, extending the resonance-dominant entanglement theory to non-Markovian and non-Hermitian optomechanical systems is also challenging and expected to be impactful. Specifically, we ensure that studying non-Markovian effects [87–91], exceptional points [92], parity-time symmetry [93], and anti-parity-time symmetry [94] on optomechanical entanglement is exciting. In particular, we are interested in future investigations of the optomechanical-entanglement properties between resonance states [95,96] in non-Hermitian systems. This work aims to develop an innovative approach for protecting continuous-variable entanglement.

ACKNOWLEDGMENTS

We are grateful to Naomichi Hatano for his inspiration and careful reading of the manuscript. C.S. took pleasure in discussions with Kinkawa Hayato. We are grateful for the feasibility suggestions provided by Chun-Hua Dong, Mai Zhang, Zhen Shen, and Yu Wang in the experimental implementation. C.S. acknowledges the financial support by the China Scholarship Council and the Japanese Government (Monbukagakusho-MEXT) Scholarship under Grant No. 211501. Additionally, C.S. would like to acknowledge the financial support provided by the RIKEN Junior Research Associate Program. H.L. is supported by the Forefront Physics and Mathematics Program to Drive Transformation (FoPM) and the World-leading Innovative Graduate Study (WINGS) program at the University of Tokyo. Additionally, we thank the referee for constructive comments that improved our work.

APPENDIX A: DERIVATION OF THE HAMILTONIAN (1)

Here, we show the origin of the total Hamiltonian (1) [46]. The total Hamiltonian (1) of this field reservoir consists of two parts, the system (2) and the environment (3). Therefore, to obtain Eq. (1), we need to demonstrate the specific origins of Eqs. (2) and (3) separately.

To begin with, we show the origin of the system Hamiltonian (2). As usual, for an optomechanical system driven by an optical laser, the Hamiltonian of the composite system can be written as

$$H_S^0 = \hbar\omega_c a^\dagger a + \frac{p'^2}{2m} + \frac{1}{2}m(\omega_m q')^2 - \hbar G a^\dagger a q' \\ + i\hbar(E e^{-i\omega_0 t} a^\dagger - E^* e^{i\omega_0 t} a), \quad (A1)$$

where a monochromatic field drives the optical mode with the driving frequency ω_0 , and the complex amplitude of the driving laser is denoted by E . The optical frequency shift per displacement is given by $G = -\partial\omega_c(x)/\partial x = \omega_c/L$. To make the Hamiltonian independent of time, we then move to the rotating frame of the frequency, which changes Eq. (A1) to the following:

$$H'_S = U(t) H_S^0(t) U^\dagger(t) - iU(t) \dot{U}^\dagger(t) \\ = \hbar\Delta_0 a^\dagger a + \frac{p'^2}{2m} + \frac{1}{2}m(\omega_m q')^2 - \hbar G a^\dagger a q' \\ + i\hbar(E a^\dagger - E^* a), \quad (A2)$$

where we used the unitary transformation of the form $U(t) = \exp(i\omega_0 a^\dagger a t)$, and $\Delta_0 = \omega_c - \omega_0$ is the detuning of the cavity characteristic frequency ω_c of the optical cavity from the driving laser frequency ω_0 .

We can make the position and momentum operators dimensionless by defining the zero-point fluctuation (ZPF) amplitude of the mechanical oscillator as $X_{\text{ZPF}} = \sqrt{\hbar/2m\omega_m}$. Then, we define the dimensionless position operator q and momentum operator p as follows:

$$q = \frac{q'}{\sqrt{2}X_{\text{ZPF}}} = \frac{1}{\sqrt{2}}(b^\dagger + b), \quad p = \frac{p'}{\sqrt{2m\omega_m X_{\text{ZPF}}}} \\ = \frac{i}{\sqrt{2}}(b^\dagger - b). \quad (A3)$$

Substituting Eq. (A3) into Eq. (A2), we arrive at

$$H_S = \hbar\Delta_0 a^\dagger a + \frac{\hbar}{2}\omega_m(p^2 + q^2) \\ - \hbar G_0 a^\dagger a q + i\hbar(E a^\dagger - E^* a) \\ = \hbar\Delta_0 a^\dagger a + \hbar\omega_m b^\dagger b - \hbar G_0 a^\dagger a \frac{(b^\dagger + b)}{\sqrt{2}} \\ + i\hbar(E a^\dagger - E^* a), \quad (A4)$$

where $G_0 = \sqrt{2}GX_{\text{ZPF}} = \omega_c\sqrt{\hbar/m\omega_m}/L$ is the vacuum optomechanical coupling strength, expressed as a frequency. It quantifies the interaction between a single phonon and a single photon. This produces Eq. (2) in the main text.

Next, we give the origin of the environment Hamiltonian (3) for the first time. As is well known from Bose-Einstein statistics, a heat bath associated with a boson system can be considered as an assembly of harmonic oscillators. This type of heat bath can serve as a model for various physical systems, such as elastic solids (mechanical reservoirs) and electromagnetic fields (optical reservoirs).

Firstly, since in the optomechanical system, both the photons in the optical cavity and the phonons in the mechanical oscillator obey Bose-Einstein statistics, the free part of the environment can be written in the simple form

$$H_E^0 = \frac{1}{2} \sum_k \left[\frac{1}{m_k^c} (\tilde{p}_k^c)^2 + \Theta_k^c (\tilde{q}_k^c)^2 \right] + \frac{1}{2} \sum_n \left[\frac{1}{m_n^m} (\tilde{p}_n^m)^2 + \Theta_n^m (\tilde{q}_n^m)^2 \right], \quad (\text{A5})$$

where m_k^c and m_n^m correspond to the effective mass of the k th optical reservoir and n th mechanical reservoir, respectively. The momentum and position operators corresponding to the k th optical reservoir and the n th mechanical reservoir are denoted by \tilde{p}_k^c (\tilde{p}_n^m) and \tilde{q}_k^c (\tilde{q}_n^m), respectively. We set $\Theta_k^c = m_k^c(\omega_k)^2$ and $\Theta_n^m = m_n^m(\omega_n)^2$ as the optical and mechanical potential-force constants. The harmonic-oscillator reservoirs have closely spaced frequencies corresponding to photons and phonons, denoted by ω_k and ω_n , respectively. Through the process of removing the dimensions from the operators, we can define the dimensionless momentum operators p_k^c and p_n^m as well as position operators q_k^c and q_n^m as follows:

$$p_k^c = \sqrt{\frac{\omega_k}{\Theta_k^c \hbar}} \tilde{p}_k^c = \sqrt{\frac{1}{m_k^c \omega_k \hbar}} \tilde{p}_k^c, \quad q_k^c = \sqrt{\frac{\Theta_k^c}{\omega_k \hbar}} \tilde{q}_k^c \\ = \sqrt{\frac{\omega_k}{\hbar}} \tilde{p}_k^c, \quad (\text{A6})$$

$$p_n^m = \sqrt{\frac{\omega_n}{\Theta_n^m \hbar}} \tilde{p}_n^m = \sqrt{\frac{1}{m_n^m \omega_n \hbar}} \tilde{p}_n^m, \quad q_n^m = \sqrt{\frac{\Theta_n^m}{\omega_n \hbar}} \tilde{q}_n^m \\ = \sqrt{\frac{\omega_n}{\hbar}} \tilde{p}_n^m. \quad (\text{A7})$$

Substituting Eqs. (A6) and (A7) into Eq. (A5), we obtain

$$H_E' = \frac{\hbar}{2} \sum_k \omega_k \left[(p_k^c)^2 + (q_k^c)^2 \right] + \frac{\hbar}{2} \sum_n \omega_n \left[(p_n^m)^2 + (q_n^m)^2 \right]. \quad (\text{A8})$$

Secondly, we consider the coupling between the system and the environment. The Hamiltonian of a system can be left arbitrary, such as an atom, as in quantum optics, or a macroscopic LC circuit. In our case, we treat the optomechanical system as a perturbation to the baths, by writing

$$H_E'' = +\frac{\hbar}{2} \sum_k \omega_k \left[(p_k^c)^2 + (q_k^c + \varepsilon_k^c q_c)^2 \right] + \frac{\hbar}{2} \sum_n \omega_n \left[(p_n^m - \chi_n^m q_m)^2 + (q_n^m)^2 \right] \\ = +\frac{\hbar}{2} \sum_k \omega_k \left[(p_k^c)^2 + (q_k^c)^2 \right] + \frac{\hbar}{2} \sum_k \omega_k (\varepsilon_k^c q_c)^2 \\ + \hbar \sum_k \omega_k \varepsilon_k^c q_k^c q_c + \frac{\hbar}{2} \sum_n \omega_n \left[(p_n^m)^2 + (q_n^m)^2 \right] \\ + \frac{\hbar}{2} \sum_n \omega_n (\chi_n^m q_m)^2 - \hbar \sum_n \omega_n \chi_n^m p_n^m q_m \quad (\text{A9})$$

or

$$\tilde{H}_E'' = +\frac{\hbar}{2} \sum_k \omega_k \left[(p_k^c + \varepsilon_k^c p_c)^2 + (q_k^c)^2 \right] + \frac{\hbar}{2} \sum_n \omega_n \left[(p_n^m - \chi_n^m q_m)^2 + (q_n^m)^2 \right] \\ = +\frac{\hbar}{2} \sum_k \omega_k \left[(p_k^c)^2 + (q_k^c)^2 \right] + \frac{\hbar}{2} \sum_k \omega_k (\varepsilon_k^c p_c)^2 \\ + \hbar \sum_k \omega_k \varepsilon_k^c p_k^c p_c + \frac{\hbar}{2} \sum_n \omega_n \left[(p_n^m)^2 + (q_n^m)^2 \right] \\ + \frac{\hbar}{2} \sum_n \omega_n (\chi_n^m q_m)^2 - \hbar \sum_n \omega_n \chi_n^m p_n^m q_m. \quad (\text{A10})$$

The orthogonal relationship for the dimensionless position and momentum operators of the system and the environment read:

$$q_c = \frac{1}{\sqrt{2}} (a^\dagger + a), \quad p_c = \frac{i}{\sqrt{2}} (a^\dagger - a); \\ q_k^c = \frac{1}{\sqrt{2}} (\Gamma_k^\dagger + \Gamma_k), \quad p_k^c = \frac{i}{\sqrt{2}} (\Gamma_k^\dagger - \Gamma_k); \quad (\text{A11})$$

$$\begin{aligned} q_m &= \frac{1}{\sqrt{2}} (b^\dagger + b), \quad p_c = \frac{i}{\sqrt{2}} (b^\dagger - b); \\ q_n^m &= \frac{1}{\sqrt{2}} (\Lambda_n^\dagger + \Lambda_n), \quad p_n^m = \frac{i}{\sqrt{2}} (\Lambda_n^\dagger - \Lambda_n). \end{aligned} \quad (\text{A12})$$

By substituting Eqs. (A11) and (A12) into Eqs. (A9) and (A10) and absorbing terms only of the system operators $\hbar \sum_k \omega_k (\varepsilon_k^c p_c)^2 / 2$, $\hbar \sum_k \omega_k (\varepsilon_k^c q_c)^2 / 2$, and $\hbar \sum_n \omega_n (\chi_n^m q_m)^2 / 2$ into the system Hamiltonian, and further neglecting these higher-order perturbation quantities containing $(\varepsilon_k^c)^2$ and $(\chi_n^m)^2$, we obtain

$$\begin{aligned} \tilde{H}_E'' \mapsto H_E^{qc} &= +\hbar \sum_k \omega_k \Gamma_k^\dagger \Gamma_k + \hbar \sum_k g_k (\Gamma_k^\dagger a^\dagger + \Gamma_k a) \\ &\quad + \hbar \sum_k g_k (\Gamma_k^\dagger a + \Gamma_k a^\dagger) + \hbar \sum_n \omega_n \Lambda_n^\dagger \Lambda_n \\ &\quad - i\hbar \sum_n \frac{\ell_n}{2} (\Lambda_n^\dagger - \Lambda_n) (b^\dagger + b), \end{aligned} \quad (\text{A13})$$

$$\begin{aligned} \tilde{H}_E'' \mapsto H_E^{pc} &= +\hbar \sum_k \omega_k \Gamma_k^\dagger \Gamma_k - \hbar \sum_k g_k (\Gamma_k^\dagger a^\dagger + \Gamma_k a) \\ &\quad + \hbar \sum_k g_k (\Gamma_k^\dagger a + \Gamma_k a^\dagger) + \hbar \sum_n \omega_n \Lambda_n^\dagger \Lambda_n \\ &\quad - i\hbar \sum_n \frac{\ell_n}{2} (\Lambda_n^\dagger - \Lambda_n) (b^\dagger + b), \end{aligned} \quad (\text{A14})$$

where we set $g_k = \varepsilon_k^c \omega_k / 2$ and $\ell_n = \chi_n^m \omega_n$. The real numbers g_k and ℓ_n represent the coupling strengths between the subsystem and the n th reservoir mode, respectively. Finally, we apply the rotating-wave approximation and neglect the counter-rotating terms $\Gamma_k^\dagger a^\dagger$ and $\Gamma_k a$ in Eqs. (A13) and (A14), yielding $H_E^{qc} \approx \tilde{H}_E^{qc} = H_E = \tilde{H}_E^{pc} \approx H_E^{pc}$, where \tilde{H}_E^{qc} and \tilde{H}_E^{pc} represent the Hamiltonians after the rotating-wave approximation. This process produces Eq. (3) in the main text.

In conclusion, we have physically revealed that photon and phonon perturbations interact with the reservoirs differently. The coupling between photons and the bosonic reservoirs results in the potential energy of the bath depending on the deviation of q_c from all the q_k^c , while the kinetic energy of the bath depends on the derivation of p_c with respect to all p_k^c as well. In other words, it is as if each coordinate q_k^c or p_k^c is harmonically bound to q_c or p_c , respectively. In contrast, the coupling between phonons and the bosonic reservoirs makes the potential energy of the bath depend on the deviation of q_m from all the p_n^m . The kinetic energy of the bath depends on the derivation of p_m with respect to all q_n^m as well. In other words, it is as if each coordinate q_n^m or p_n^m is harmonically bound to p_m or q_m , respectively.

In addition, we point out that this difference between perturbations of photons and phonons on the bosonic reservoirs also results in the fact that, in the rotating-wave approximation, neglecting the rotating-wave terms $\Gamma_k^\dagger a^\dagger$ and $\Gamma_k a$ in the coupling between photons and the electromagnetic field leads to the simplification $\sum_k \omega_k [(p_k^c + \varepsilon_k^c p_c)^2 + (q_k^c)^2] \approx \sum_k \omega_k [(p_k^c)^2 + (q_k^c + \varepsilon_k^c q_c)^2]$, while neglecting the counter-rotating terms $\Lambda_n^\dagger b$ and $\Lambda_n b^\dagger$ in the coupling between phonons and the elastic solid simplifies $\sum_n \omega_n [(p_n^m - \chi_n^m q_m)^2 + (q_n^m)^2] \approx \sum_n \omega_n [(p_n^m)^2 + (q_n^m - \chi_n^m p_m)^2]$.

APPENDIX B: DETAILS OF THE DERIVATION OF Eqs. (4)–(6)

In this appendix, we derive the nonlinear Langevin equations that the total Hamiltonian H_T in Eq. (1) satisfies. To begin with, let us derive the nonlinear Langevin equations satisfied by the optical cavity field. The Heisenberg equations of motion for the operator a of the optical cavity field and its corresponding reservoir operators Γ_k are given by

$$\begin{aligned} \dot{a} &= \frac{1}{i\hbar} [a, H_T] = -i\Delta_0 a + iG_0 a \frac{(b^\dagger + b)}{\sqrt{2}} \\ &\quad + E - i \sum_k g_k \Gamma_k, \end{aligned} \quad (\text{B1})$$

$$\dot{\Gamma}_k = \frac{1}{i\hbar} [\Gamma_k, H_T] = -i\omega_k \Gamma_k - ig_k a. \quad (\text{B2})$$

We are interested in a closed equation for a . Equation (B2) for Γ_k can be formally integrated to yield

$$\Gamma_k(t) = \Gamma_k(t_0) e^{-i\omega_k(t-t_0)} - ig_k \int_{t_0}^t a(\tau) e^{-i\omega_k(t-\tau)} d\tau. \quad (\text{B3})$$

Here the first term describes the free evolution of the reservoir modes, whereas the second term arises from their interaction with the optical cavity field. We eliminate Γ_k by substituting Eq. (B3) into Eq. (B1), finding

$$\begin{aligned} \dot{a} &= -i\Delta_0 a + iG_0 a \frac{(b^\dagger + b)}{\sqrt{2}} + E \\ &\quad - \sum_k (g_k)^2 \int_{t_0}^t a(\tau) e^{-i\omega_k(t-\tau)} d\tau + f_a(t), \end{aligned} \quad (\text{B4})$$

with $f_a(t) = -i \sum_k g_k \Gamma_k(t_0) \exp[-i\omega_k(t-t_0)]$. In Eq. (B4), we can see that the evolution of the system operator depends on the fluctuations in the reservoir.

To proceed, we introduce some approximations. Following the Weisskopf-Wigner approximation [49], we replace

the summation over k in Eq. (B4) with an integral term, thereby transitioning from a discrete distribution of modes to a continuous one, $\sum_k \mapsto (L/2\pi)^3 \int d^3k$, where L is the length of the sides of the assumed cubic cavity with no specific boundaries, and $\vec{k} \equiv (k_x, k_y, k_z)$ is the wave vector.

The density of modes between the frequencies ω and $\omega + d\omega$ can be obtained by transferring from Cartesian coordinates to polar coordinates as

$$\begin{aligned}\vec{k} \equiv (k_x, k_y, k_z) &\mapsto [k \sin(\theta) \cos(\phi), \\ &k \sin(\theta) \sin(\phi), k \cos(\theta)].\end{aligned}$$

The corresponding volume element in \vec{k} space is

$$d^3k = k^2 \sin(\theta) dk d\theta d\phi = (\omega^2/c^3) \sin(\theta) d\omega d\theta d\phi.$$

The total number of modes N_a in the range between ω and $\omega + d\omega$ is given by

$$\begin{aligned}dN_a &= (L/2\pi c)^3 \omega^2 d\omega \int_0^\pi \sin(\theta) d\theta \int_0^{2\pi} d\phi \\ &= (L^3 \omega^2 / 2\pi^2 c^3) d\omega.\end{aligned}$$

A mode density parameter at frequency ω is therefore given by $D_a(\omega) = dN_a(\omega)/d\omega = L^3 \omega^2 / 2\pi^2 c^3$, and $g_k = g[k(\omega)] = g(\omega)$ is the coupling constant evaluated at $k = \omega/c$. We then approximate this spectrum by a continuous spectrum.

Thus, the summation in Eq. (B4) can be written as

$$\begin{aligned}\dot{a} &= -i\Delta_0 a + iG_0 a \frac{(b^\dagger + b)}{\sqrt{2}} + E \\ &- \int_{t_0}^t \int_0^{+\infty} g^2(\omega) D_a(\omega) e^{-i\omega(t-\tau)} a(\tau) d\omega d\tau + f_a(t).\end{aligned}\quad (B5)$$

Considering an ideal situation, we assume for simplicity that $[g(\omega)]^2 D_a(\omega) = \kappa/\pi > 0$ is constant, so that Eq. (B5) is reduced to a simple first-order differential equation [51]:

$$\begin{aligned}\dot{a} &= -i\Delta_0 a + iG_0 a \frac{(b^\dagger + b)}{\sqrt{2}} + E \\ &- \frac{\kappa}{\pi} \int_{t_0}^{t+0^+} \int_0^{+\infty} e^{-i\omega(t-\tau)} a(\tau) d\omega d\tau + f_a(t).\end{aligned}\quad (B6)$$

Using the relation

$$\int_0^{+\infty} e^{-i\omega(t-\tau)} d\omega = \pi \delta(t - \tau), \quad (B7)$$

we arrive at Eq. (6) in the main text:

$$\dot{a} = -(\kappa + i\Delta_0) a + iG_0 a \frac{(b^\dagger + b)}{\sqrt{2}} + E + \sqrt{2\kappa} a_{\text{in}} \quad (B8)$$

with

$$a_{\text{in}}(t) = \frac{f_a(t)}{\sqrt{2\kappa}} = \frac{-i}{\sqrt{2\pi}} \sum_k g_k \Gamma(t_0) e^{-i\omega_k(t-t_0)}, \quad (B9)$$

where $a_{\text{in}}(t)$ is a noise operator, which depends upon the environment operators $\Gamma(t_0)$ at the initial time, and κ is the decay rate of the optical cavity field, which depends on the coupling strength g_k of the optical cavity field and its corresponding reservoirs. We have $q = (b^\dagger + b)/\sqrt{2}$ (quadrature definition), and thus we obtain

$$\dot{a} = -(\kappa + i\Delta_0) a + iG_0 a q + E + \sqrt{2\kappa} a_{\text{in}}. \quad (B10)$$

Similarly, the Heisenberg equations of motion for the mechanical operator b and its corresponding reservoir operators Λ_n are given by

$$\begin{aligned}\dot{b} &= \frac{1}{i\hbar} [b, H_T] = -i\omega_m b + i \frac{G_0}{\sqrt{2}} a^\dagger a \\ &- \frac{1}{2} \sum_n \ell_n (\Lambda_n^\dagger - \Lambda_n),\end{aligned}\quad (B11)$$

$$\begin{aligned}\dot{b}^\dagger &= \frac{1}{i\hbar} [b^\dagger, H_T] = i\omega_m b^\dagger - i \frac{G_0}{\sqrt{2}} a^\dagger a \\ &+ \frac{1}{2} \sum_n \ell_n (\Lambda_n^\dagger - \Lambda_n),\end{aligned}\quad (B12)$$

$$\dot{\Lambda}_n = \frac{1}{i\hbar} [\Lambda_n, H_T] = -i\omega_n \Lambda_n - \ell_n \frac{(b^\dagger + b)}{2}, \quad (B13)$$

$$\dot{\Lambda}_n^\dagger = \frac{1}{i\hbar} [\Lambda_n^\dagger, H_T] = i\omega_n \Lambda_n - \ell_n \frac{(b^\dagger + b)}{2}. \quad (B14)$$

Since we have the orthogonal relationship, $q = (b^\dagger + b)/\sqrt{2}$ and $p = i(b^\dagger - b)/\sqrt{2}$, where p and q are the dimensionless position and momentum operators of the mirror that satisfy the commutation relation $[q, p] = i$. The derivatives of q and p with respect to time read

$$\dot{q} = \frac{1}{\sqrt{2}} (\dot{b}^\dagger + \dot{b}) = \omega_m p, \quad (B15)$$

$$\begin{aligned}\dot{p} &= \frac{i}{\sqrt{2}} (\dot{b}^\dagger - \dot{b}) = -\omega_m q + G_0 a^\dagger a \\ &+ i \sum_n \ell_n \frac{(\Lambda_n^\dagger - \Lambda_n)}{\sqrt{2}}.\end{aligned}\quad (B16)$$

Equation (B15) corresponds to Eq. (4) in the main text.

We now focus on a closed equation for p . Equations (B13) and (B14) for Λ_n and Λ_n^\dagger can be formally integrated to yield

$$\begin{aligned}\Lambda_n(t) &= \Lambda_n(t_0) e^{-i\omega_n(t-t_0)} - \frac{1}{2} \ell_n \int_{t_0}^t [b^\dagger(\tau) + b(\tau)] \\ &\times e^{-i\omega_n(t-\tau)} d\tau,\end{aligned}\quad (\text{B17})$$

$$\begin{aligned}\Lambda_n^\dagger(t) &= \Lambda_n^\dagger(t_0) e^{i\omega_n(t-t_0)} - \frac{1}{2} \ell_n \int_{t_0}^t [b^\dagger(\tau) + b(\tau)] \\ &\times e^{i\omega_n(t-\tau)} d\tau.\end{aligned}\quad (\text{B18})$$

We then eliminate the reservoir operators Λ_n and Λ_n^\dagger by substituting Eqs. (B17) and (B18) into Eq. (B16), and obtain

$$\dot{p} = -\omega_m q + G_0 a^\dagger a + \Theta + \xi, \quad (\text{B19})$$

where

$$\xi(t) = \frac{i}{\sqrt{2}} \sum_n \ell_n [\Lambda_n^\dagger(t_0) e^{i\omega_n(t-t_0)} - \Lambda_n(t_0) e^{-i\omega_n(t-t_0)}] \quad (\text{B20})$$

and

$$\Theta(t) = \sum_n (\ell_n)^2 \int_{t_0}^t q(\tau) \sin[\omega_n(t-\tau)] d\tau. \quad (\text{B21})$$

Equation (B20) is the same as Eq. (8) in the main text [54, 97].

We then integrate Eq. (B21) by parts and obtain

$$\begin{aligned}\Theta(t) &= \sum_n \frac{(\ell_n)^2}{\omega_n} \{q(t) \cos[\omega_n(t-t_0)]\}_{t_0}^t \\ &- \sum_n \frac{(\ell_n)^2}{\omega_n} \int_{t_0}^t \dot{q}(\tau) \cos[\omega_n(t-\tau)] d\tau.\end{aligned}\quad (\text{B22})$$

The integrand function $\varsigma(t) = \sum_n [(\ell_n)^2 \cos(\omega_n t)]/\omega_n$ can be seen to have the form of a memory function since it makes the equation of motion at time t depend on the values of $\dot{q}(t)$ for the previous time. Within the Born-Markov approximation [98], we consider that $\varsigma(t)$ is a rapidly decaying function and that the equation has a short memory. More precisely, if $\varsigma(t)$ goes to zero in a time scale that is much less than the time over which $\dot{q}(t)$ changes, then we can replace $\dot{q}(\tau)$ by $\dot{q}(t)$. For t not close to the initial

time t_0 , we can drop the first term in Eq. (B22). Thus, Eq. (B22) reads

$$\Theta(t) \approx - \sum_n \frac{(\ell_n)^2}{\omega_n} \int_{t_0}^t \dot{q}(\tau) \cos[\omega_n(t-\tau)] d\tau. \quad (\text{B23})$$

Similarly to the optical cavity mode a , using the Weisskopf-Wigner approximation, we consider the spectrum to be given by the normal modes of a large scale, $L \rightarrow +\infty$. A difference between phonons and photons is that $g_k = g[k(\omega)] = g(\omega)$ is the coupling constant evaluated at $\omega \propto k^2$. We then approximate this spectrum by a continuous spectrum. Thus, the summation in Eq. (B23) can be written as

$$\Theta(t) \approx - \int_0^{+\infty} \int_{t_0}^t d\omega d\tau \frac{[\ell(\omega)]^2}{\omega} \dot{q}(\tau) \cos[\omega(t-\tau)] D_b(\omega). \quad (\text{B24})$$

Considering an ideal situation, by setting $[\ell(\omega)]^2 D_b(\omega)/\omega = \gamma/\pi$, we thereby obtain

$$\Theta(t) \approx -\frac{\gamma}{\pi} \int_0^{+\infty} \int_{t_0}^{t+0^+} d\omega d\tau \dot{q}(\tau) \cos[\omega(t-\tau)]. \quad (\text{B25})$$

Using the relations

$$\int_0^{+\infty} \cos[\omega(t-\tau)] d\omega = \pi \delta(t-\tau), \quad (\text{B26})$$

and by substituting Eq. (B15) into $\Theta(t) \approx -\gamma \dot{q}(t)$, we arrive at Eq. (5) in the main text:

$$\dot{p} = -\omega_m q - \gamma_m p + G_0 a^\dagger a + \xi, \quad (\text{B27})$$

where the mechanical damping rate is $\gamma_m = \omega_m \gamma$, which depends on the coupling strength ℓ_n and the characteristic frequency of the mechanical oscillator ω_m .

APPENDIX C: DETAILED DESCRIPTION OF THE HIGH-FREQUENCY INVERSE-RESONANCE REGION

In our work, we mainly focus on discussing the high-frequency resonance range since its physical significance is clear and universal. However, the high-frequency inverse-resonance range does indeed exist and holds a specific physical meaning, as explained below.

A high-frequency inverse-resonance range requires a heat bath consisting of harmonic oscillators with negative-energy modes. Such oscillators are equivalent to those with negative mass, which have been studied in schemes to evade quantum measurement back-action [99, 100]. Such a

scheme was experimentally demonstrated using an atomic spin ensemble initially in its maximal-energy spin state within a magnetic field. Spin flips decrease the energy and correspond to excitations of a harmonic oscillator with a negative mass [101]. Alternatively, a frame rotating faster than the mode itself can effectively realize the negative-energy mode, such as quantum back-action evading measurement of collective mechanical modes [102,103]. In our setup, a heat bath with negative frequencies can be implemented through engineering dissipation in a multimode optomechanical circuit [34,104,105].

We consider a mechanical mode coherently coupled to a heat bath comprising negative-energy modes in the inverse-resonance region $\omega_m(\lambda) \omega_n(\lambda) \leq 0$, which is described by the Hamiltonian

$$H = \hbar \sum_n \omega_n(\lambda) \Lambda_n^\dagger \Lambda_n + \hbar \omega_m(\lambda) b^\dagger b - i\hbar \sum_n \frac{\ell_n}{2} (\Lambda_n^\dagger - \Lambda_n) (b^\dagger + b), \quad (C1)$$

with the same symbols as defined in the main text. Here the bare frequencies $\omega_n(\lambda) \leq 0$ and $\omega_m(\lambda) \geq 0$ vary with respect to a parameter λ . To achieve filter design, we introduce a frequency transformation

$$\begin{aligned} \tilde{\Lambda}_n(t) &= \Lambda_n(t) \exp[-i|\omega_n(\lambda)|t] \quad \text{and} \quad \tilde{b}(t) \\ &= b(t) \exp[i\omega_m(\lambda)t] \end{aligned} \quad (C2)$$

for $\Lambda_n(t)$ and $b(t)$ in the interaction picture [49].

After the transformation, it becomes clear that the mechanical mode has a positive phase (i.e., counterclockwise rotation), whereas its corresponding heat-bath mode exhibits a negative phase (i.e., clockwise rotation). In the presence of high-frequency inverse-resonance dominance, we effectively eliminate the terms $\tilde{\Lambda}_n \tilde{b}^\dagger$ and $\tilde{\Lambda}_n^\dagger \tilde{b}$ associated with high-frequency oscillations. After the filtering process, we keep only the terms of $\tilde{\Lambda}_n^\dagger \tilde{b}^\dagger$ and $\tilde{\Lambda}_n \tilde{b}$, and hence Eq. (C1) becomes

$$H' = -\hbar \sum_n |\omega_n(\lambda)| \Lambda_n^\dagger \Lambda_n + \hbar \omega_m(\lambda) b^\dagger b - i\hbar \sum_n \frac{\ell_n}{2} (\Lambda_n^\dagger b^\dagger - \Lambda_n b), \quad (C3)$$

which satisfies a typical coupling form between a positive-energy mode and negative-energy modes.

Despite the negative frequency of the heat-bath mode implying a negative mean thermal phonon number, it does harbor intriguing physical features, namely level attraction [60]. Without loss of generality, now let us show it by two minimal models. The first one is for the usual level repulsion of two coherently coupled positive-energy

modes (the high-frequency resonance region, namely a general red-detuned regime, wherein the dominant term is $-i\hbar\ell_1(\Lambda_1^\dagger b - \Lambda_1 b^\dagger)/2$, which describes the exchange of quanta between them [18]). The other one is for level attraction of a negative-energy mode coherently coupled to a positive-energy mode (the high-frequency inverse-resonance region, namely a general blue-detuned regime, wherein the dominant term is $-i\hbar\ell_1(\Lambda_1^\dagger b^\dagger - \Lambda_1 b)/2$, which represents a two-mode squeezing interaction that lies at the heart of parametric amplification [61]). There is a symmetry relation linking the two cases, as they are images of each other.

First, we derive level repulsion (LR) of two coupled positive-energy modes with an energy crossing, which has applications ranging from solid-state theory to quantum chemistry. Two modes of positive energy interact, as described by the Hamiltonian [60]

$$\begin{aligned} H_{\text{LR}} &= \hbar |\omega_1(\lambda)| \Lambda_1^\dagger \Lambda_1 + \hbar \omega_m(\lambda) b^\dagger b \\ &- i\hbar \frac{\ell_1}{2} (\Lambda_1^\dagger b - \Lambda_1 b^\dagger). \end{aligned} \quad (C4)$$

The equation of motion in the Heisenberg picture is given by

$$\frac{d}{dt} \begin{pmatrix} \Lambda_1 \\ b \end{pmatrix} = -i \begin{pmatrix} |\omega_1| & \frac{1}{2}i\ell_1 \\ -\frac{1}{2}i\ell_1 & \omega_m \end{pmatrix} \begin{pmatrix} \Lambda_1 \\ b \end{pmatrix}. \quad (C5)$$

The hybridized eigenmodes $\tilde{\omega}_{\text{LR}}$ of the system are obtained by diagonalizing the coefficient matrix in Eq. (C5), and have eigenfrequencies

$$\omega_{\text{LR}}^\pm = \frac{1}{2} \left\{ |\omega_1| + \omega_m \pm \sqrt{(|\omega_1| - \omega_m)^2 + \ell_1^2} \right\}, \quad (C6)$$

where we drop the explicit λ dependence.

We now consider level attraction (LA). A negative-energy mode is coherently coupled to a positive-energy mode such that the system is described by the Hamiltonian

$$\begin{aligned} H_{\text{LA}} &= -\hbar |\omega_1(\lambda)| \Lambda_1^\dagger \Lambda_1 + \hbar \omega_m(\lambda) b^\dagger b \\ &- i\hbar \frac{\ell_1}{2} (\Lambda_1^\dagger b^\dagger - \Lambda_1 b). \end{aligned} \quad (C7)$$

The equation of motion in the Heisenberg picture is given by

$$\frac{d}{dt} \begin{pmatrix} \Lambda_1 \\ b^\dagger \end{pmatrix} = i \begin{pmatrix} |\omega_1| & \frac{1}{2}i\ell_1 \\ \frac{1}{2}i\ell_1 & \omega_m \end{pmatrix} \begin{pmatrix} \Lambda_1 \\ b^\dagger \end{pmatrix}, \quad (C8)$$

with the eigenmodes $\tilde{\omega}_{\text{LA}}$ and the corresponding eigenfrequencies

$$\omega_{\text{LA}}^\pm = \frac{1}{2} \left\{ |\omega_1| + \omega_m \pm \sqrt{(|\omega_1| - \omega_m)^2 - \ell_1^2} \right\}, \quad (C9)$$

where we drop the explicit λ dependence.

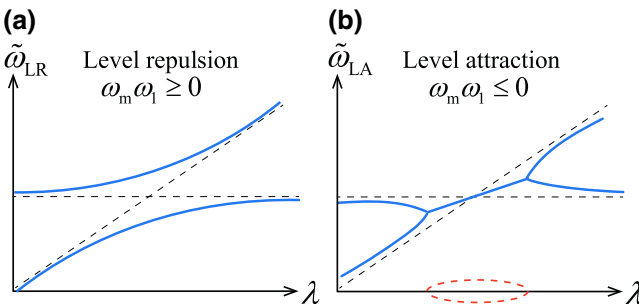


FIG. 8. Level repulsion and attraction are characterized by ω_1 [60]. Two modes, whose bare frequencies depend on a parameter λ , have a level crossing (dashed lines). When a coherent coupling is introduced, it generally lifts the degeneracy between these modes, leading to distinct behaviors. (a) In the more common scenario of level repulsion, the coupling opens a gap between the frequencies of the hybridized eigenmodes $\tilde{\omega}_{\text{LR}}$ (blue solid lines) and the eigenfrequencies ω_{LR}^{\pm} bend away from each other. (b) In contrast, in the case of level attraction, where one mode exhibits negative energy, level attraction occurs. The real components of the eigenfrequencies $\tilde{\omega}_{\text{LA}}^{\pm}$ (blue solid lines) bend toward each other, converging at two exceptional points marked by kinks. Simultaneously, finite imaginary components of the frequencies emerge (orange dashed lines). Notably, the mode with a negative imaginary component becomes unstable, exhibiting exponential growth.

The only difference between Eqs. (C6) and (C9) is the sign in front of ℓ_1^2 . However, that dramatically impacts the physics. The Hermitian Hamiltonian (C7) can result in a complex eigenvalue and unstable dynamics, in which the eigenoperators cannot be interpreted as Bogoliubov modes [106]. We depict the repulsion and attraction of levels in Fig. 8. In contrast to the level repulsion (C4), the level attraction (C7) has two prominent features. First, the eigenfrequencies are drawn toward each other instead of avoiding each other. Second, to satisfy the condition $(|\omega_1(\lambda)| - \omega_m)^2 = \ell_1^2$, the frequencies acquire negative and positive imaginary parts, leading to exponential growth and decay. Thus, the heat bath consisting of a group of harmonic oscillators with negative modes in Hamiltonian (C3) exhibits instability. Furthermore, we observe that the level attraction arises when the coupling term includes a Pauli matrix with an imaginary coefficient.

In the case of level attraction, the interaction term can be expressed as $i\ell_1\sigma_x/2$ by decomposing it in terms of Pauli matrices and omitting the term proportional to the identity. In contrast, in the case of level repulsion, the interaction term would be $-\ell_1\sigma_y/2$. In addition, we decompose the coefficient matrix in Eq. (C8) into $[(|\omega_1| - \omega_m)\sigma_z + i\ell_1\sigma_x]/2$. If the first term has a larger amplitude, the eigenfrequencies are real, while they are complex if the second term dominates. It is worth noting that when two Pauli matrices have coefficients of the same amplitude, the matrix is proportional to $\sigma_z + i\sigma_x$. At this

point, the two eigenvectors coalesce, and a single eigenvector with a single eigenvalue subsists, is marked by an exceptional point and corresponds to the point of maximal nonreciprocity, which can lead to a nonreciprocal photon transmission and amplification via reservoir engineering [107]. More details are explained in Ref. [60]. To sum up, we have shown that the negative frequency of the heat bath holds a particular and significant physical meaning. Firstly, the quantum back-action evading measurement of collective mechanical modes provides the possibility to prepare an ensemble of effective negative-mass oscillators. Secondly, negative-energy modes coupled with a positive mode, having opposite phases between a mechanical mode and modes of the heat bath, can lead to an intriguing level attraction of complex spectra associated with exceptional points and unstable dynamics.

APPENDIX D: DETAILS OF THE DERIVATION OF Eqs. (11) AND (12)

In this appendix, we focus on deriving the nonlinear Langevin equations satisfied by the filtering model H_F under the dominance of resonance effects. Specifically, we concentrate on the mechanical mode b , keeping the optical cavity mode a in the same form as the dynamical equation (6). By substituting the filtering model H_F into the Heisenberg equation, we obtain

$$\dot{b} = \frac{1}{i\hbar} [b, H_T] = -i\omega_m b + i\frac{G_0}{\sqrt{2}} a^\dagger a + \frac{1}{2} \sum_n \ell_n \Lambda_n, \quad (\text{D1})$$

$$\dot{b}^\dagger = \frac{1}{i\hbar} [b^\dagger, H_T] = i\omega_m b^\dagger - i\frac{G_0}{\sqrt{2}} a^\dagger a + \frac{1}{2} \sum_n \ell_n \Lambda_n^\dagger, \quad (\text{D2})$$

$$\dot{\Lambda}_n = \frac{1}{i\hbar} [\Lambda_n, H_F] = -i\omega_n \Lambda_n - \frac{\ell_n}{2} b, \quad (\text{D3})$$

$$\dot{\Lambda}_n^\dagger = \frac{1}{i\hbar} [\Lambda_n^\dagger, H_F] = i\omega_n \Lambda_n^\dagger - \frac{\ell_n}{2} b^\dagger. \quad (\text{D4})$$

The derivatives of p and q with respect to time read

$$\dot{q} = \frac{1}{\sqrt{2}} (\dot{b}^\dagger + \dot{b}) = \omega_m p + \frac{1}{2} \sum_n \ell_n q_n, \quad (\text{D5})$$

$$\dot{p} = \frac{i}{\sqrt{2}} (\dot{b}^\dagger - \dot{b}) = -\omega_m q + G_0 a^\dagger a + \frac{1}{2} \sum_n \ell_n p_n. \quad (\text{D6})$$

We are interested in the system operators p and q . Equations (D3) and (D4) for Λ_n and Λ_n^\dagger can be formally

integrated to yield

$$\Lambda_n(t) = \Lambda_n(t_0) e^{-i\omega_n(t-t_0)} - \frac{\ell_n}{2} \int_{t_0}^t b(\tau) e^{-i\omega_n(t-\tau)} d\tau, \quad (\text{D7})$$

$$\Lambda_n^\dagger(t) = \Lambda_n^\dagger(t_0) e^{i\omega_n(t-t_0)} - \frac{\ell_n}{2} \int_{t_0}^t b^\dagger(\tau) e^{i\omega_n(t-\tau)} d\tau. \quad (\text{D8})$$

The parts of Eqs. (D5) and (D6) that contain environmental operators q_n and p_n can be written as

$$\begin{aligned} \frac{1}{2} \sum_n \ell_n q_n &= \frac{1}{2} \sum_n \ell_n \frac{\Lambda_n^\dagger + \Lambda_n}{\sqrt{2}} = \frac{1}{2} \sum_n \ell_n \frac{1}{\sqrt{2}} \\ &\times [\Lambda_n^\dagger(t_0) e^{i\omega_n(t-t_0)} + \Lambda_n(t_0) e^{-i\omega_n(t-t_0)}] \\ &- \sum_n \left(\frac{\ell_n}{2} \right)^2 \frac{1}{\sqrt{2}} \left[\int_{t_0}^t b^\dagger(\tau) e^{i\omega_n(t-\tau)} d\tau \right. \\ &\left. + \int_{t_0}^t b(\tau) e^{-i\omega_n(t-\tau)} d\tau \right], \end{aligned} \quad (\text{D9})$$

$$\begin{aligned} \frac{1}{2} \sum_n \ell_n p_n &= \frac{1}{2} \sum_n \ell_n \frac{i(\Lambda_n^\dagger - \Lambda_n)}{\sqrt{2}} = \frac{1}{2} \sum_n \ell_n \frac{i}{\sqrt{2}} \\ &[\Lambda_n^\dagger(t_0) e^{i\omega_n(t-t_0)} - \Lambda_n(t_0) e^{-i\omega_n(t-t_0)}] \\ &- \sum_n \left(\frac{\ell_n}{2} \right)^2 \frac{i}{\sqrt{2}} \left[\int_{t_0}^t b^\dagger(\tau) e^{i\omega_n(t-\tau)} d\tau \right. \\ &\left. - \int_{t_0}^t b(\tau) e^{-i\omega_n(t-\tau)} d\tau \right]. \end{aligned} \quad (\text{D10})$$

For convenience, we concisely express Eqs. (D9) and (D10) as

$$\frac{1}{2} \sum_n \ell_n q_n = \frac{1}{2} \xi'(t) - \chi'(t), \quad (\text{D11})$$

$$\frac{1}{2} \sum_n \ell_n p_n = \frac{1}{2} \xi(t) - \chi(t), \quad (\text{D12})$$

where

$$\xi'(t) = \sum_n \ell_n \frac{1}{\sqrt{2}} [\Lambda_n^\dagger(t_0) e^{i\omega_n(t-t_0)} + \Lambda_n(t_0) e^{-i\omega_n(t-t_0)}], \quad (\text{D13})$$

$$\xi(t) = \sum_n \ell_n \frac{i}{\sqrt{2}} [\Lambda_n^\dagger(t_0) e^{i\omega_n(t-t_0)} - \Lambda_n(t_0) e^{-i\omega_n(t-t_0)}], \quad (\text{D14})$$

$$\begin{aligned} \chi'(t) &= \sum_n \left(\frac{\ell_n}{2} \right)^2 \int_{t_0}^t \{q(\tau) \cos[\omega_n(t-\tau)] \right. \\ &\left. + p(\tau) \sin[\omega_n(t-\tau)]\} d\tau, \end{aligned} \quad (\text{D15})$$

$$\begin{aligned} \chi(t) &= \sum_n \left(\frac{\ell_n}{2} \right)^2 \int_{t_0}^t \{p(\tau) \cos[\omega_n(t-\tau)] \right. \\ &\left. - q(\tau) \sin[\omega_n(t-\tau)]\} d\tau. \end{aligned} \quad (\text{D16})$$

Next, we make some approximations. In a similar way to Appendix B, under the Born-Markov and Weisskopf-Wigner approximations, Eqs. (D15) and (D16) become

$$\begin{aligned} \chi'(t) &= \frac{1}{4} \int_0^{+\infty} \int_{t_0}^{t+0^+} d\tau d\omega \{\dot{q}(t) \sin[\omega(t-\tau)] \\ &- \dot{p}(t) \cos[\omega(t-\tau)]\} \frac{[\ell(\omega)]^2 D_b(\omega)}{\omega}, \end{aligned} \quad (\text{D17})$$

$$\begin{aligned} \chi(t) &= \frac{1}{4} \int_0^{+\infty} \int_{t_0}^{t+0^+} d\tau d\omega \{\dot{p}(t) \sin[\omega(t-\tau)] \\ &+ \dot{q}(t) \cos[\omega(t-\tau)]\} \frac{[\ell(\omega)]^2 D_b(\omega)}{\omega}. \end{aligned} \quad (\text{D18})$$

Furthermore, we set $[\ell(\omega)]^2 D_b(\omega)/\omega = \gamma/\pi$. Then, by using the relation $\int_0^{+\infty} \cos[\omega(t-\tau)] d\omega = \pi \delta(t-\tau)$ and $\int_0^{+\infty} \sin[\omega(t-\tau)] d\omega = 0$, we find $\chi'(t) = -\gamma \dot{p}(t)/4$ and $\chi(t) = \gamma \dot{q}(t)/4$.

Finally, Eqs. (D5) and (D6) can be rewritten as

$$\dot{q} = \omega_m p + \frac{\gamma}{4} \dot{p} + \frac{1}{2} \xi', \quad (\text{D19})$$

$$\dot{p} = -\omega_m q - \frac{\gamma}{4} \dot{q} + G_0 a^\dagger a + \frac{1}{2} \xi(t). \quad (\text{D20})$$

We ultimately reproduce the same equations as Eqs. (11) and (12) presented in the main text.

APPENDIX E: DETAILS OF THE DERIVATION OF Eqs. (15)–(17)

We set the mechanical damping rate as $\gamma_m = \omega_m \gamma$. For the part of the quantum fluctuation operators, we have

$$\delta \dot{q} = \omega_m \delta p + \frac{\gamma}{4} \delta \dot{p} + \frac{1}{2} \xi', \quad (\text{E1})$$

$$\delta \dot{p} = -\omega_m \delta q - \frac{\gamma}{4} \delta \dot{q} + G_0 (\alpha_s^* \delta a + \alpha_s \delta a^\dagger + \delta a \delta a^\dagger) + \frac{1}{2} \xi, \quad (\text{E2})$$

$$\begin{aligned} \delta \dot{a} &= -(\kappa + i\Delta_0) \delta a + iG_0 (\alpha_s \delta q + q_s \delta a + \delta a \delta q) \\ &+ \sqrt{2\kappa} a_{\text{in}}. \end{aligned} \quad (\text{E3})$$

To decouple $\delta\dot{q}$ and $\delta\dot{p}$, by substituting Eqs. (E1) and (E2) into each other, we obtain

$$\begin{aligned} \left(1 + \frac{\gamma^2}{16}\right)\delta\dot{q} &= \omega_m\delta p - \frac{\gamma_m}{4}\delta q + \frac{1}{2}\xi' + \frac{\gamma G_0}{4}(\alpha_s^*\delta a + \alpha_s\delta a^\dagger + \delta a\delta a^\dagger) + \frac{1}{8}\gamma\xi, \\ \left(1 + \frac{\gamma^2}{16}\right)\delta\dot{p} &= -\omega_m\delta q - \frac{\gamma_m}{4}\delta p + G_0(\alpha_s^*\delta a + \alpha_s\delta a^\dagger) + \frac{1}{2}\xi + G_0\delta a\delta a^\dagger - \frac{1}{8}\gamma\xi', \\ \delta\dot{a} &= -(\kappa + i\Delta)\delta a + iG_0\alpha_s\delta q + \sqrt{2\kappa}a_{\text{in}} + iG_0\delta a\delta q, \end{aligned} \quad (\text{E4})$$

where $\gamma_m = \gamma\omega_m$. By dropping the second-order small terms, we obtain the linearized Langevin equations

$$\delta\dot{q} = \omega_m\delta p - \frac{\gamma_m}{4}\delta q + \frac{1}{2}\xi', \quad (\text{E5})$$

$$\delta\dot{p} = -\omega_m\delta q - \frac{\gamma_m}{4}\delta p + G_0(\alpha_s^*\delta a + \alpha_s\delta a^\dagger) + \frac{1}{2}\xi, \quad (\text{E6})$$

$$\delta\dot{a} = -(\kappa + i\Delta)\delta a + iG_0\alpha_s\delta q + \sqrt{2\kappa}a_{\text{in}}, \quad (\text{E7})$$

which are consistent with Eqs. (15)–(17) in the main text.

APPENDIX F: DETAILS OF THE DERIVATION OF THE LYAPUNOV EQUATION

This appendix derives the Lyapunov equation $A V + V A^T + D = 0$. We begin with the definition of the covariance matrix. According to the definition [108], any matrix element of the covariance matrix can be expressed as

$$V_{ij}(t) = \frac{1}{2}\langle\mu_i(t)\mu_j(t) + \mu_j(t)\mu_i(t)\rangle, \quad (\text{F1})$$

which satisfies the differential equation

$$\frac{dV_{ij}(t)}{dt} = \frac{1}{2}\left\langle \frac{d\mu_i(t)}{dt}\mu_j(t) + \mu_i(t)\frac{d\mu_j(t)}{dt} + \frac{d\mu_j(t)}{dt}\mu_i(t) + \mu_j(t)\frac{d\mu_i(t)}{dt} \right\rangle. \quad (\text{F2})$$

The matrix elements of the differential equation (F2) read

$$\dot{\mu}_i(t) = \sum_r A_{ir}\mu_r(t) + n_i(t). \quad (\text{F3})$$

Substituting Eq. (F3) into Eq. (F2), we obtain

$$\begin{aligned} \frac{dV_{ij}(t)}{dt} &= +\frac{1}{2}\left\langle \left[\sum_r A_{ir}\mu_r(t) + n_i(t) \right] \mu_j(t) + \mu_i(t) \left[\sum_r A_{jr}\mu_r(t) + n_j(t) \right] \right\rangle \\ &\quad + \frac{1}{2}\left\langle \left[\sum_r A_{jr}\mu_r(t) + n_j(t) \right] \mu_i(t) + \mu_j(t) \left[\sum_r A_{ir}\mu_r(t) + n_i(t) \right] \right\rangle \\ &= \sum_r A_{ir}(t)V_{rj}(t) + \sum_r A_{jr}(t)V_{ir}(t) + D_{ij}(t), \end{aligned} \quad (\text{F4})$$

where

$$D_{ij}(t) = \frac{\langle n_i(t)\mu_j(t) \rangle + \langle \mu_i(t)n_j(t) \rangle + \langle n_j(t)\mu_i(t) \rangle + \langle \mu_j(t)n_i(t) \rangle}{2}. \quad (\text{F5})$$

We then calculate each term in D_{ij} . For example, we have

$$\begin{aligned}\langle n_i(t) \mu_j(t) \rangle &= \left\langle n_i(t) \sum_r \left[M_{jr}(t, t_0) \mu_r(t_0) + \int_{t_0}^t M_{jr}(t, \tau) n_r(\tau) d\tau \right] \right\rangle \\ &= \sum_r M_{jr}(t, t_0) \langle n_i(t) \mu_r(t_0) \rangle + \sum_r \int_{t_0}^t M_{jr}(t, \tau) \langle n_i(t) n_j(\tau) \rangle d\tau \\ &= \sum_r \int_{t_0}^t M_{jr}(t, \tau) \langle n_i(t) n_j(\tau) \rangle d\tau,\end{aligned}\quad (\text{F6})$$

where $M(t) = \exp(At)$. Similarly, we obtain the other terms in D_{ij} , which are

$$\langle \mu_i(t) n_j(t) \rangle = \sum_r \int_{t_0}^t M_{ir}(t, \tau) \langle n_r(\tau) n_j(t) \rangle d\tau, \quad (\text{F7})$$

$$\langle n_j(t) \mu_i(t) \rangle = \sum_r \int_{t_0}^t M_{ir}(t, \tau) \langle n_j(t) n_r(\tau) \rangle d\tau, \quad (\text{F8})$$

$$\langle \mu_j(t) n_i(t) \rangle = \sum_r \int_{t_0}^t M_{jr}(t, \tau) \langle n_r(\tau) n_i(t) \rangle d\tau. \quad (\text{F9})$$

Hence, D_{ij} can be written as

$$D_{ij} = \sum_r \int_{t_0}^t M_{jr}(t, \tau) \Phi_{ir}^{(1)}(t, \tau) d\tau + \sum_r \int_{t_0}^t M_{ir}(t, \tau) \Phi_{rj}^{(2)}(t, \tau) d\tau, \quad (\text{F10})$$

where

$$\Phi_{ir}^{(1)}(t, \tau) = \frac{1}{2} \langle n_i(t) n_r(\tau) + n_r(\tau) n_i(t) \rangle, \quad (\text{F11})$$

$$\Phi_{rj}^{(2)}(t, \tau) = \frac{1}{2} \langle n_r(\tau) n_j(t) + n_j(t) n_r(\tau) \rangle. \quad (\text{F12})$$

The transposes of the column vector of noise operators are given by $n^T(t) = [0.5\xi'(t), 0.5\xi(t), \sqrt{2\kappa}X_{\text{in}}(t), \sqrt{2\kappa}Y_{\text{in}}(t)]$. We note that the nonzero correlation functions satisfy the following relations:

$$2 \langle X_{\text{in}}(t) Y_{\text{in}}(\tau) \rangle = -2 \langle Y_{\text{in}}(t) X_{\text{in}}(\tau) \rangle = -i\delta(t - \tau), \quad (\text{F13})$$

$$2 \langle X_{\text{in}}(t) X_{\text{in}}(\tau) \rangle = 2 \langle Y_{\text{in}}(t) Y_{\text{in}}(\tau) \rangle = (2\bar{n}_a + 1) \delta(t - \tau), \quad (\text{F14})$$

$$\langle \xi(t) \xi(\tau) + \xi(\tau) \xi(t) \rangle = \langle \xi'(t) \xi'(\tau) + \xi'(\tau) \xi'(t) \rangle = 2\gamma_m (2\bar{n} + 1) \delta(t - \tau). \quad (\text{F15})$$

To be concise, we set \bar{n}_a equal to zero. Using the relations (F13)–(F15), we calculate each term of $\Phi_{ir}^{(1)}(t, \tau)$ and $\Phi_{rj}^{(2)}(t, \tau)$. The result is given by

$$\Phi_{ir}^{(1)} = \begin{pmatrix} \Phi_{11}^{(1)} & \Phi_{12}^{(1)} & \Phi_{13}^{(1)} & \Phi_{14}^{(1)} \\ \Phi_{21}^{(1)} & \Phi_{22}^{(1)} & \Phi_{23}^{(1)} & \Phi_{24}^{(1)} \\ \Phi_{31}^{(1)} & \Phi_{32}^{(1)} & \Phi_{33}^{(1)} & \Phi_{34}^{(1)} \\ \Phi_{41}^{(1)} & \Phi_{42}^{(1)} & \Phi_{43}^{(1)} & \Phi_{44}^{(1)} \end{pmatrix} = D_{ir} \delta(t - \tau), \quad (\text{F16})$$

where $D_{ir} = \text{diag}[\gamma_m (2\bar{n} + 1)/4, \gamma_m (2\bar{n} + 1)/4, \kappa, \kappa]$.

Similarly, we obtain $\Phi_{rj}^{(2)} = D_{rj} \delta(t - \tau) = \text{diag}[\gamma_m (2\bar{n} + 1)/4, \gamma_m (2\bar{n} + 1)/4, \kappa, \kappa] \delta(t - \tau)$. Therefore, Eq. (F10) can be rewritten as

$$\begin{aligned} D_{ij} &= \sum_r \int_{t_0}^t M_{jr}(t, \tau) \Phi_{ir}^{(1)}(\tau) d\tau + \sum_r \int_{t_0}^t M_{ir}(t, \tau) \Phi_{rj}^{(2)}(\tau) d\tau \\ &= \sum_r \int_{t_0}^t M_{jr}(t, \tau) D_{ir} \delta(t - \tau) d\tau + \sum_r \int_{t_0}^t M_{ir}(t, \tau) D_{rj} \delta(t - \tau) d\tau \\ &= \frac{1}{2} \sum_r I_{jr} D_{ir} + \frac{1}{2} \sum_r I_{ir} D_{rj} = \frac{1}{2} \sum_r D_{ir} I_{rj}^T + \frac{1}{2} \sum_r I_{ir} D_{rj} = D, \end{aligned} \quad (\text{F17})$$

where $D = \text{diag}[\gamma_m (2\bar{n} + 1)/4, \gamma_m (2\bar{n} + 1)/4, \kappa, \kappa]$.

Hence, we obtain

$$A V = \int_{t_0}^{\infty} A M(\tau) D M(\tau)^T d\tau = \int_{t_0}^{\infty} \frac{d}{d\tau} M(\tau) D M(\tau)^T d\tau, \quad (\text{F18})$$

$$V A^T = \int_{t_0}^{\infty} M(\tau) D (A M(\tau))^T d\tau = \int_{t_0}^{\infty} M(\tau) D \frac{d}{d\tau} M(\tau)^T d\tau. \quad (\text{F19})$$

The combination of Eqs. (F18) and (F19) becomes

$$A V + V A^T = + \int_{t_0}^{\infty} \frac{d}{d\tau} [M(\tau) D M(\tau)^T] d\tau - \int_{t_0}^{\infty} M(\tau) \frac{d}{d\tau} D M(\tau)^T d\tau = [M(\tau) D M(\tau)^T] \Big|_{t_0}^{+\infty} = -D. \quad (\text{F20})$$

When the stability conditions are satisfied, in the long-time limit, the derivative of the covariance matrix with respect to time approaches zero, $\dot{V} = 0$, and the solution $M(+\infty)$ converges to zero. This produces the Lyapunov equation in the main text, $A V + V A^T = -D$.

-
- [1] E. Schrödinger, Die gegenwärtige Situation in der Quantenmechanik, *Sci. Nat.* **23**, 807 (1935).
 - [2] J. S. Bell, On the Einstein Podolsky Rosen paradox, *Phys. Phys. Fiz.* **1**, 195 (1964).
 - [3] D. Bouwmeester, A. Ekert, and A. Zeilinger, *The Physics of Quantum Information* (Springer, Berlin, 2000).
 - [4] F. J. Duarte and T. Taylor, *Quantum Entanglement Engineering and Applications* (IOP Press, London, 2021).
 - [5] A. Streltsov, G. Adesso, and M. B. Plenio, Colloquium: Quantum coherence as a resource, *Rev. Mod. Phys.* **89**, 041003 (2017).
 - [6] S. Takeda, M. Fuwa, P. van Loock, and A. Furusawa, Entanglement Swapping between Discrete and Continuous Variables, *Phys. Rev. Lett.* **114**, 100501 (2015).
 - [7] G. Masada, K. Miyata, A. Politi, T. Hashimoto, J. L. O'Brien, and A. Furusawa, Continuous-variable entanglement on a chip, *Nat. Photonics* **9**, 316 (2015).
 - [8] D. Estève, J.-M. Raimond, and J. Dalibard, *Quantum Entanglement and Information Processing* (Elsevier, Amsterdam, 2003).
 - [9] W. K. Wootters, Entanglement of Formation of an Arbitrary State of Two Qubits, *Phys. Rev. Lett.* **80**, 2245 (1998).

- [10] A. Miranowicz and A. Grudka, Ordering two-qubit states with concurrence and negativity, *Phys. Rev. A* **70**, 032326 (2004).
- [11] I. Bengtsson and K. Życzkowski, *Geometry of Quantum States: An Introduction to Quantum Entanglement* (Cambridge University Press, UK, 2006).
- [12] V. Vedral, Quantifying entanglement in macroscopic systems, *Nature* **453**, 1004 (2008).
- [13] L.-M. Duan, G. Giedke, J. I. Cirac, and P. Zoller, Entanglement Purification of Gaussian Continuous Variable Quantum States, *Phys. Rev. Lett.* **84**, 4002 (2000).
- [14] W. P. Bowen, R. Schnabel, P. K. Lam, and T. C. Ralph, Experimental Investigation of Criteria for Continuous Variable Entanglement, *Phys. Rev. Lett.* **90**, 043601 (2003).
- [15] S. P. Walborn, B. G. Taketani, A. Salles, F. Toscano, and R. L. de Matos Filho, Entropic Entanglement Criteria for Continuous Variables, *Phys. Rev. Lett.* **103**, 160505 (2009).
- [16] R. Horodecki, P. Horodecki, M. Horodecki, and K. Horodecki, Quantum entanglement, *Rev. Mod. Phys.* **81**, 865 (2009).
- [17] C. M. Caves, Quantum-Mechanical Radiation-Pressure Fluctuations in an Interferometer, *Phys. Rev. Lett.* **45**, 75 (1980).

- [18] M. Aspelmeyer, T. J. Kippenberg, and F. Marquardt, Cavity optomechanics, *Rev. Mod. Phys.* **86**, 1391 (2014).
- [19] A. Bachtold, J. Moser, and M. I. Dykman, Mesoscopic physics of nanomechanical systems, *Rev. Mod. Phys.* **94**, 045005 (2022).
- [20] M. Aspelmeyer, P. Meystre, and K. Schwab, Quantum optomechanics, *Phys. Today* **65**(7), 29 (2012).
- [21] M. Aspelmeyer, T. J. Kippenberg, and F. Marquardt, *Cavity Optomechanics: Nano- and Micromechanical Resonators Interacting with Light* (Springer, Germany, 2014).
- [22] Y. H. Zhou, H. Z. Shen, and X. X. Yi, Unconventional photon blockade with second-order nonlinearity, *Phys. Rev. A* **92**, 023838 (2015).
- [23] H. Z. Shen, Y. H. Zhou, and X. X. Yi, Tunable photon blockade in coupled semiconductor cavities, *Phys. Rev. A* **91**, 063808 (2015).
- [24] M. Trupke, E. A. Hinds, S. Eriksson, E. A. Curtiss, Z. Mokhtadir, E. Kukharenka, M. Trupke, E. A. Hinds, and M. Kraft, Microfabricated high-finesse optical cavity with open access and small volume, *Appl. Phys. Lett.* **87**, 211106 (2005).
- [25] H. Z. Shen, Y. H. Zhou, and X. X. Yi, Quantum optical diode with semiconductor microcavities, *Phys. Rev. A* **90**, 023849 (2014).
- [26] S. L. Braunstein and P. van Loock, Quantum information with continuous variables, *Rev. Mod. Phys.* **77**, 513 (2005).
- [27] M. A. Macovei and A. Pálffy, Multiphonon quantum dynamics in cavity optomechanical systems, *Phys. Rev. A* **105**, 033503 (2022).
- [28] D. Vitali, S. Gigan, A. Ferreira, H. R. Böhm, P. Tombesi, A. Guerreiro, V. Vedral, A. Zeilinger, and M. Aspelmeyer, Optomechanical Entanglement between a Movable Mirror and a Cavity Field, *Phys. Rev. Lett.* **98**, 030405 (2007).
- [29] K. Y. Dixon, L. Cohen, N. Bhusal, C. Wipf, J. P. Dowling, and T. Corbitt, Optomechanical entanglement at room temperature: A simulation study with realistic conditions, *Phys. Rev. A* **102**, 063518 (2020).
- [30] M. B. Plenio, Logarithmic Negativity: A Full Entanglement Monotone That Is Not Convex, *Phys. Rev. Lett.* **95**, 090503 (2005).
- [31] D.-G. Lai, J.-Q. Liao, A. Miranowicz, and F. Nori, Noise-Tolerant Optomechanical Entanglement via Synthetic Magnetism, *Phys. Rev. Lett.* **129**, 063602 (2022).
- [32] J.-X. Liu, Y.-F. Jiao, Y. Li, X.-W. Xu, Q.-Y. He, and H. Jing, Phased-controlled asymmetric optomechanical entanglement against optical backscattering, *Sci. China Phys. Mech. Astron.* **66**, 230312 (2023).
- [33] Y.-F. Jiao, S.-D. Zhang, Y.-L. Zhang, A. Miranowicz, L.-M. Kuang, and H. Jing, Nonreciprocal Optomechanical Entanglement against Backscattering Losses, *Phys. Rev. Lett.* **125**, 143605 (2020).
- [34] Cheng Shang, H. Z. Shen, and X. X. Yi, Nonreciprocity in a strong coupled three-mode optomechanical circulatory system, *Opt. Express* **27**, 18 (2019).
- [35] J. Huang, D.-G. Lai, and J.-Q. Liao, Thermal-noise-resistant optomechanical entanglement via general dark-mode control, *Phys. Rev. A* **106**, 063506 (2022).
- [36] G. D. Chiara, M. Paternostro, and G. M. Palma, Entanglement detection in hybrid optomechanical systems, *Phys. Rev. A* **83**, 052324 (2011).
- [37] L. Zhou, Y. Han, J. T. Jing, and W. P. Zhang, Entanglement of nanomechanical oscillators and two-mode fields induced by atomic coherence, *Phys. Rev. A* **83**, 052117 (2011).
- [38] C. Shang, Coupling enhancement and symmetrization of single-photon optomechanics in open quantum systems, *ArXiv:2302.04897*.
- [39] M. Bekele, T. Yirgashewa, and S. Tesfa, Entanglement of mechanical modes in a doubly resonant optomechanical cavity of a correlated emission laser, *Phys. Rev. A* **107**, 012417 (2003).
- [40] M. Bekele, T. Yirgashewa, and S. Tesfa, Effects of a three-level laser on mechanical squeezing in a doubly resonant optomechanical cavity coupled to biased noise fluctuations, *Phys. Rev. A* **105**, 053502 (2022).
- [41] Y.-Q Shi, L. Cong, and H.-P. Eckle, Entanglement resonance in the asymmetric quantum Rabi model, *Phys. Rev. A* **105**, 062450 (2022).
- [42] R. Ghobadi, S. Kumar, B. Pepper, D. Bouwmeester, A. I. Lvovsky, and C. Simon, Optomechanical Micro-Macro Entanglement, *Phys. Rev. Lett.* **112**, 080503 (2014).
- [43] C. Gut, K. Winkler, J. H.-Obermaier, S. G. Hofer, R. M. Nia, N. Walk, A. Steffens, J. Eisert, W. Wieczorek, J. A. Slater, M. Aspelmeyer, and K. Hammerer, Stationary optomechanical entanglement between a mechanical oscillator and its measurement apparatus, *Phys. Rev. Res.* **2**, 033244 (2020).
- [44] J. Kohler, N. Spethmann, S. Schreppler, and D. M. S.-Kurn, Cavity-Assisted Measurement and Coherent Control of Collective Atomic Spin Oscillators, *Phys. Rev. Lett.* **118**, 063604 (2017).
- [45] H. Y. Sun, Cheng Shang, X. X. Luo, Y. H. Zhou, and H. Z. Shen, Optical-assisted photon blockade in a cavity system via parametric interactions, *Int. J. Theor. Phys.* **58**, 3640 (2019).
- [46] T. A. Palomaki, J. D. Teufel, R. W. Simmonds, and K. W. Lehnert, Entangling mechanical motion with microwave fields, *Science* **342**, 710 (2013).
- [47] J. Chan, T. P. M. Alegre, A. H. Safavi-Naeini, J. T. Hill, A. Krause, S. Groeblacher, M. Aspelmeyer, and O. Painter, Laser cooling of a nanomechanical oscillator into its quantum ground state, *Nature* **478**, 89 (2011).
- [48] A. A. Rakhubovsky and R. Filip, Robust entanglement with a thermal mechanical resonator, *Phys. Rev. A* **91**, 062317 (2015).
- [49] M. O. Scully and M. S. Zubairy, *Quantum Optics* (Cambridge University Press, UK, 2011).
- [50] C. K. Law, Interaction between a moving mirror and radiation pressure: A Hamiltonian formulation, *Phys. Rev. A* **51**, 2537 (1995).
- [51] C. W. Gardiner and P. Zoller, *Quantum Noise* (Springer, Berlin, 2000).
- [52] Y.-L. Liu, R. Wu, J. Zhang, S. K. Özdemir, L. Yang, F. Nori, and Y.-X. Liu, Controllable optical response by modifying the gain and loss of a mechanical resonator and

- cavity mode in an optomechanical system, *Phys. Rev. A* **95**, 013843 (2017).
- [53] V. Giovannetti and D. Vitali, Phase-noise measurement in a cavity with a movable mirror undergoing quantum Brownian motion, *Phys. Rev. A* **63**, 023812 (2001).
- [54] R. Benguria and M. Kac, Quantum Langevin Equation, *Phys. Rev. Lett.* **46**, 1 (1981).
- [55] Z.-G. Lu, C. Shang, Y. Wu, and X.-Y. Lü, Analytical approach to higher-order correlation function in U(1) symmetric systems, *ArXiv:2305.08923*.
- [56] R. Alicki, Master equations for a damped nonlinear oscillator and the validity of the Markovian approximation, *Phys. Rev. A* **40**, 4077 (1989).
- [57] D. Antonio, D. H. Zanette, and D. López, Frequency stabilization in nonlinear micromechanical oscillators, *Nat. Commun.* **3**, 806 (2012).
- [58] E. Verhagen, S. Deléglise, S. Weis, A. Schliesser, and T. J. Kippenberg, Quantum-coherent coupling of a mechanical oscillator to an optical cavity mode, *Nature* **482**, 63 (2012).
- [59] N. W. Ashcroft and N. David Mermin, *Solid State Physics* (Brooks Cole, New York, 1976).
- [60] N. R. Bernier, L. D. Tóth, A. K. Feofanov, and T. J. Kippenberg, Level attraction in a microwave optomechanical circuit, *Phys. Rev. A* **98**, 023841 (2018).
- [61] A. A. Clerk, M. H. Devoret, S. M. Girvin, F. Marquardt, and R. J. Schoelkopf, Introduction to quantum noise, measurement, and amplification, *Rev. Mod. Phys.* **82**, 1155 (2010).
- [62] G. Adesso, A. Serafini, and F. Illuminati, Extremal entanglement and mixedness in continuous variable systems, *Phys. Rev. A* **70**, 022318 (2004).
- [63] E. Knill, R. Laflamme, and G. J. Milburn, A scheme for efficient quantum computation with linear optics, *Nature* **409**, 46 (2001).
- [64] E. X. DeJesus and C. Kaufman, Routh-Hurwitz criterion in the examination of eigenvalues of a system of nonlinear ordinary differential equations, *Phys. Rev. A* **35**, 5288 (1987).
- [65] G. Vidal and R. P. Werner, Computable measure of entanglement, *Phys. Rev. A* **65**, 032314 (2002).
- [66] C. Weedbrook, S. Pirandola, R. G. Patrón, N. J. Cerf, T. C. Ralph, J. H. Shapiro, and S. Lloyd, Gaussian quantum information, *Rev. Mod. Phys.* **84**, 621 (2012).
- [67] R. Simon, Peres-Horodecki Separability Criterion for Continuous Variable Systems, *Phys. Rev. Lett.* **84**, 2726 (2000).
- [68] S. Gigan, H. R. Böhm, M. Paternostro, F. Blaser, G. Langer, J. B. Hertzberg, K. C. Schwab, D. Bäuerle, M. Aspelmeyer, and A. Zeilinger, Self-cooling of a micromirror by radiation pressure, *Nature* **444**, 67 (2006).
- [69] O. Arcizet, P.-F. Cohadon, T. Briant, M. Pinard, and A. Heidmann, Radiation-pressure cooling and optomechanical instability of a micromirror, *Nature* **444**, 71 (2006).
- [70] D. Kleckner and D. Bouwmeester, Sub-kelvin optical cooling of a micromechanical resonator, *Nature* **444**, 75 (2006).
- [71] D. Kleckner, W. Marshall, M. J. A. de Dood, K. N. Dinyari, B.-J. Ports, W. T. M. Irvine, and D. Bouwmeester, High Finesse Opto-Mechanical Cavity with a Movable Thirty-Micron-Size Mirror, *Phys. Rev. Lett.* **96**, 173901 (2006).
- [72] W. Xiong, D.-Y. Jin, Y. Qiu, C.-H. Lam, and J. Q. You, Cross-Kerr effect on an optomechanical system, *Phys. Rev. A* **93**, 023844 (2016).
- [73] T. A. Palomaki, J. D. Teufel, R. W. Simmonds, and K. W. Lehnert, Entangling mechanical motion with microwave fields, *Science* **10**, 1126 (2013).
- [74] T. A. Palomaki, J. W. Harlow, J. D. Teufel, R. W. Simmonds, and K. W. Lehnert, Coherent state transfer between itinerant microwave fields and a mechanical oscillator, *Nature* **495**, 210 (2013).
- [75] J. R. Johansson, G. Johansson, and F. Nori, Optomechanical-like coupling between superconducting resonators, *Phys. Rev. A* **90**, 053833 (2014).
- [76] H. X. Miao, S. Danilishin, and Y. B. Chen, Universal quantum entanglement between an oscillator and continuous fields, *Phys. Rev. A* **81**, 052307 (2010).
- [77] S. Gröblacher, A. Trubarov, N. Prigge, G. D. Cole, M. Aspelmeyer, and J. Eisert, Observation of non-Markovian micromechanical Brownian motion, *Nat. Commun.* **6**, 7606 (2015).
- [78] G. Cariolaro and R. Corvaja, Implementation of two-mode Gaussian states whose covariance matrix has the standard form, *Symmetry* **14**, 1485 (2022).
- [79] J. Laurat, G. Keller, J. A. O.-Huguenin, C. Fabre, T. Coudreau, A. Serafini, G. Adesso, and F. Illuminati, Entanglement of two-mode Gaussian states: Characterization and experimental production and manipulation, *J. Opt. B* **7**, S577 (2005).
- [80] J. S. Xu, C. F. Li, X. Y. Xu, C. H. Shi, X. B. Zou, and G. C. Guo, Experimental Characterization of Entanglement Dynamics in Noisy Channels, *Phys. Rev. Lett.* **103**, 240502 (2009).
- [81] B. H. Liu, L. Li, Y. F. Huang, C. F. Li, G. C. Guo, E. M. Laine, H. P. Breuer, and J. Piilo, Experimental control of the transition from Markovian to non-Markovian dynamics of open quantum systems, *Nat. Phys.* **7**, 931 (2011).
- [82] L. Mancino, M. Sbroscia, I. Gianani, E. Roccia, and M. Barbieri, Quantum Simulation of Single-Qubit Thermometry Using Linear Optics, *Phys. Rev. Lett.* **118**, 130502 (2017).
- [83] J. S. Xu, M. H. Yung, X. Y. Xu, S. Boixo, Z. W. Zhou, C. F. Li, A. Aspuru-Guzik, and G. C. Guo, Demon-like algorithmic quantum cooling and its realization with quantum optics, *Nat. Photonics* **8**, 113 (2014).
- [84] K. Bartkiewicz, A. Černoch, K. Lemr, A. Miranowicz, and F. Nori, Experimental temporal quantum steering, *Sci. Rep.* **6**, 38076 (2016).
- [85] S.-J. Xiong, Y. Zhang, Z. Sun, L. Yu, Q. Su, X.-Q. Xu, J.-S. Jin, Q. Xu, J.-M. Liu, K. Chen, and C.-P. Yang, Experimental simulation of a quantum channel without the rotating-wave approximation: Testing quantum temporal steering, *Optica* **4**, 1065 (2017).
- [86] S. G. Mokarzel, A. N. Salgueiro, and M. C. Nemes, Modeling the reversible decoherence of mesoscopic superpositions in dissipative environments, *Phys. Rev. A* **65**, 044101 (2002).

- [87] K.-L. Liu and H.-S. Goan, Non-Markovian entanglement dynamics of quantum continuous variable systems in thermal environments, *Phys. Rev. A* **76**, 022312 (2007).
- [88] F. F. Fanchini, T. Werlang, C. A. Brasil, L. G. E. Arruda, and A. O. Caldeira, Non-Markovian dynamics of quantum discord, *Phys. Rev. A* **81**, 052107 (2010).
- [89] H. Z. Shen, Cheng Shang, and X. X. Yi, Unconventional single-photon blockade in non-Markovian systems, *Phys. Rev. A* **98**, 023856 (2018).
- [90] I. D. Vega and D. Alonso, Dynamics of non-Markovian open quantum systems, *Rev. Mod. Phys.* **89**, 015001 (2017).
- [91] Y.-H. Zhou, X.-Y. Zhang, T. Liu, Q.-C. Wu, Z.-C. Shi, H.-Z. Shen, and C.-P. Yang, Environmentally induced photon blockade via two-photon absorption, *Phys. Rev. Appl.* **18**, 064009 (2022).
- [92] P. Djorwe, Y. Pennec, and B. D.-Rouhani, Frequency locking and controllable chaos through exceptional points in optomechanics, *Phys. Rev. E* **98**, 032201 (2018).
- [93] C. M. Bender, Making sense of non-Hermitian Hamiltonians, *Rep. Prog. Phys.* **70**, 947 (2007).
- [94] X.-W. Luo, C. W. Zhang, and S. W. Du, Quantum Squeezing and Sensing with Pseudo-Anti-Parity-Time Symmetry, *Phys. Rev. Lett.* **128**, 173602 (2022).
- [95] G. Ordóñez and N. Hatano, The arrow of time in open quantum systems and dynamical breaking of the resonance-anti-resonance symmetry, *J. Phys. A: Math Theor.* **50**, 405304 (2017).
- [96] N. Hatano, What is the resonant state in open quantum systems, *J. Phys.: Conf. Ser.* **2038**, 012013 (2021).
- [97] K. Jacobs, I. Tittonen, H. M. Wiseman, and S. Schiller, Quantum noise in the position measurement of a cavity mirror undergoing Brownian motion, *Phys. Rev. A* **60**, 1 (1999).
- [98] G. M. Moy, J. J. Hope, and C. M. Savage, Born and Markov approximations for atom lasers, *Phys. Rev. A* **59**, 667 (1999).
- [99] M. Tsang and C. M. Caves, Evading Quantum Mechanics, *Phys. Rev. X* **2**, 031016 (2012).
- [100] K. Zhang, P. Meystre, and W. Zhang, Back-action-free quantum optomechanics with negative-mass Bose-Einstein condensates, *Phys. Rev. A* **88**, 043632 (2013).
- [101] C. B. Møller, R. A. Thomas, G. Vasilakis, E. Zeuthen, Y. Tsaturyan, M. Balabas, K. Jensen, A. Schliesser, K. Hammerer, and E. S. Polzik, Quantum back-action-evading measurement of motion in a negative mass reference frame, *Nature* **547**, 191 (2017).
- [102] M. J. Woolley and A. A. Clerk, Two-mode back-action-evading measurements in cavity optomechanics, *Phys. Rev. A* **87**, 063846 (2013).
- [103] C. F. Ockeloen-Korppi, E. Damskägg, J.-M. Pirkkalainen, A. A. Clerk, M. J. Woolley, and M. A. Sillanpää, Quantum Back-Action Evading Measurement of Collective Mechanical Modes, *Phys. Rev. Lett.* **117**, 140401 (2016).
- [104] N. R. Bernier, L. D. Tóth, A. Koottandavida, M. A. Ioannou, D. Malz, A. Nunnenkamp, A. K. Feofanov, and T. J. Kippenberg, Nonreciprocal reconfigurable microwave optomechanical circuit, *Nat. Phys.* **13**, 787 (2017).
- [105] J. D. Teufel, D. Li, M. S. Allman, K. Cicak, A. J. Sirois, J. D. Whittaker, and R. W. Simmonds, Circuit cavity electromechanics in the strong-coupling regime, *Nature* **471**, 204 (2011).
- [106] A. L. Fetter and J. D. Walecka, *Quantum Theory of Many-Particle Systems* (Dover Books on Physics, New York, 2003).
- [107] A. Metelmann and A. A. Clerk, Nonreciprocal Photon Transmission and Amplification via Reservoir Engineering, *Phys. Rev. X* **5**, 021025 (2015).
- [108] M. Paternostro, D. Vitali, S. Gigan, M. S. Kim, C. Brukner, J. Eisert, and M. Aspelmeyer, Creating and Probing Multipartite Macroscopic Entanglement with Light, *Phys. Rev. Lett.* **99**, 250401 (2007).